JM PAPERS

Poiseuille and thermal transpiration flows of a dense gas between two parallel plates

Masanari Hattori[1,2]†

[1]Department of Aeronautics and Astronautics, Graduate School of Engineering, Kyoto University, Kyoto 615-8540, Japan

[2]Research Project of Fluid Science and Engineering, Advanced Engineering Research Center, Kyoto University, Kyoto 615-8540, Japan

The Poiseuille and thermal transpiration flows of a dense gas between two parallel plates are investigated on the basis of the Enskog kinetic equation under the diffuse reflection boundary condition. In contrast to the case of an ideal gas, the density and the gradients of pressure and the normal stress component in the flow direction are not uniform in the direction normal to the plates for a dense gas. The non-uniform normal stress gradient contributes also to the acceleration or deceleration of the thermal transpiration flow for small Knudsen numbers. The profiles of mass and heat flows as well as the net mass flows are obtained for various Knudsen numbers and ratios of the molecular diameter to the distance of plates. In the analysis of the Poiseuille flow, most characteristics of a force-driven flow with a small force are recovered. However, for the case of a dense gas, differences between the force-driven and the present pressure-driven flows are observed even within the linearized regime for small force and pressure gradient, especially at the microscopic level. The behaviour of the velocity distribution functions, in particular, the way in which they approach the ones for the Boltzmann equation as the molecular diameter becomes smaller, is clarified.

Key words: kinetic theory, non-continuum effects

1. Introduction

Gases in small systems, such as porous media with small pores and micro and nanodevices, cannot be described properly by conventional fluid dynamics. This is because the mean free path of gas molecules can be comparable to the characteristic length of system so that the underlying assumption that the gas is very close to the local equilibrium breaks

† Email address for correspondence: hattori.masanari.4r@kyoto-u.ac.jp

down due to insufficient intermolecular collisions. The kinetic theory of gases is required to describe their behaviour correctly.

Generally, the solution of the Boltzmann equation, the governing equation in the kinetic theory, is a formidable task since, besides a time and a position, the molecular velocity also plays a role of independent variable and the term representing the effect of intermolecular collisions (the collision integral) is complicated. As for its numerical solution method, both the stochastic direct simulation Monte Carlo (DSMC) method (see, e.g. Bird 1994) and deterministic methods (see, e.g. Dimarco & Pareschi 2014, and the references therein) have been developed continuously from earlier times. Owing to the continuous efforts of many researchers, there is a huge accumulation of results for the flows of ideal gases these days (see, e.g. Cercignani 1988; Sone 2007) which are described by the Boltzmann equation. There are a large number of kinetic theory studies on classical problems in fluid dynamics such as the Poiseuille flow, the Couette flow, etc. and those on phenomena peculiar to non-equilibrium gases such as the thermal transpiration flow, which is induced by a temperature gradient along a channel wall in the absence of an external force and a pressure gradient.

Meanwhile, when gases become dense, they exhibit non-ideal gas effects. Kinetic theory descriptions are available also for this case. The Enskog equation, which can describe effects owing to the finite size of molecules such as the excluded volume, and its extension, the Enskog–Vlasov equation, in which long-range interactions are dealt with by a collective mean field, have been widely accepted. Because the finite size of molecules is taken into account in the Enskog collision integral, it is more complicated than the Boltzmann collision integral. For these equations, the DSMC method was successfully constructed more than two decades ago (Montanero & Santos 1996; Frezzotti 1997). Then, using this method Frezzotti and co-workers have conducted many studies on liquid–vapour systems based on the Enskog–Vlasov equation (see, e.g. Frezzotti, Gibelli & Lorenzani 2005; Frezzotti, Barbante & Gibelli 2019).

Besides the liquid–vapour systems, the dense gas effects become relevant in small systems, such as nanoporous media, which has been activating the recent kinetic theory studies (see, e.g. Wu *et al.* 2016; Sheng *et al.* 2020; Shan *et al.* 2021). In these studies, the competition of system characteristic length, mean free path and molecular diameter is focused on, and its effect on the phenomena is investigated. This trend may be due to related applications such as shale gas extraction, where the pressure is high and the characteristic length is short, and to the fact that deterministic numerical computations are becoming feasible thanks to the extension of the fast Fourier spectral method (Filbet, Mouhot & Pareschi 2006) to the Enskog equation (Wu, Zhang & Reese 2015). However, all of the aforementioned works concentrate on the force-driven Poiseuille flow, and currently, no other type of flow seems to be investigated at the same level.

Under these circumstances, a time-dependent heat transfer in a dense gas between two parallel plates was investigated in Hattori, Tanaka & Takata (2022) and interesting features such as the effect of the finite molecular size on the propagation of disturbance were demonstrated. In the present work, we newly consider the thermal transpiration flow as well as the pressure-driven Poiseuille flow of a dense gas between two parallel plates. Analysis of these flows for the case of a rarefied gas is a fundamental problem in the kinetic theory (see, e.g. Cercignani & Daneri 1963; Cercignani & Sernagiotto 1966; Niimi 1968; Sone & Yamamoto 1968; Loyalka 1971; Niimi 1971; Hasegawa & Sone 1988; Ohwada, Sone & Aoki 1989; Loyalka & Hamoodi 1990; Kosuge *et al.* 2005; Takata & Funagane 2011; Funagane & Takata 2012). We investigate the counterpart problem for

a dense gas. We clarify how finite-size effects of molecules affect these flows, thereby aiming to contribute to increased understanding of the dense gas flow characteristics.

The paper is organized as follows. In § 2, the problem is stated and formulated. The problem is reduced to the spatially one-dimensional boundary-value problems of the linearized Enskog equation for the Poiseuille and thermal transpiration flows, in which the ratio of the mean free path and that of the molecular diameter to the distance between the plates are included as non-dimensional parameters characterizing the smallness of the system and denseness of the gas. Then, the numerical method is briefly explained in § 3. The method is an iteration based on the integral formulation of the Enskog equation combined with the fast Fourier spectral method for the computation of the collision integral. Section 4 presents the numerical results, where we show the behaviour of the macroscopic quantities (gradients of pressure and stress and profiles of density and mass/heat flow) as well as the velocity distribution functions (VDFs). Comparison between the force-driven and the present pressure-driven Poiseuille flows is also carried out. Section 5 concludes the paper.

2. Formulation

2.1. *Problem and assumptions*

Consider a dense gas between two parallel plates at rest located respectively at $X_1 = \pm D/2$, where X_i are the Cartesian coordinates. The two plates are kept at the temperature $T_w(X_2) = T_0(1 + c_T X_2/D)$ ($c_T = (D/T_0)(\mathrm{d}T_w/\mathrm{d}X_2)$ is a constant), and the gas is subject to some pressure gradient in the X_2 direction. We will find a solution that has a pressure gradient that is constant in the X_2 direction (but non-constant in the X_1 direction). There is no external force acting on the gas. The average density of the gas over the cross-section $X_2 = 0$ is given by ρ_0. We will investigate the steady behaviour of the gas under the assumptions that (i) the behaviour of the gas can be described by the Enskog equation for hard-sphere molecules with a common diameter σ and mass m with the factor of pair correlation being given according to the Carnahan–Starling equation of state (Carnahan & Starling 1969); (ii) the gas molecules are diffusely reflected on the surface of the plates; (iii) the magnitudes of the applied temperature gradient $|c_T|$ and the pressure gradient $(D/p_0)|\partial p/\partial X_2|$ are so small that the equation and boundary condition can be linearized around the state that is achieved when both gradients are absent (p is the pressure, $p_0 = \rho_0 R T_0$ and R is the specific gas constant).

Some comments on the appropriateness of the linearization assumption (iii) may be in order. At a glance, the assumption might look restrictive to describe the flows well. However, (a) the pressure and temperature gradients can in fact be small in small systems like micro/nano channels and porous media with small pores; (b) the assumption is actually employed also in the literature (see, e.g. any references cited in the third sentence of the fifth paragraph in § 1); (c) it is reported (see, e.g. Ohwada *et al.* 1989; Sharipov 2003; Ewart *et al.* 2007) that the results for rarefied gases obtained based on the linearized Boltzmann or model kinetic equations agree well with experimental results for a wide range of the Knudsen number. Based on these facts, the assumption is also employed here for the Enskog equation. Phenomena due to nonlinear effects, expected to be significant when the applied pressure or temperature gradient is not small, e.g. non-uniformity of temperature profile in pressure-driven flow (Zheng, Garcia & Alder 2002), are outside of the scope of the present work.

2.2. *Basic equation and boundary condition*

Let us denote by $X = Dx$ the position, by $(2RT_0)^{1/2}\boldsymbol{\zeta}$ the molecular velocity, by $\rho_0(2RT_0)^{-3/2}\hat{f}$ the VDF of gas molecules, by $\sigma = D\hat{\sigma}$ the molecular diameter, by $\rho_0\hat{\rho}$ the density of the gas and by $T_w = T_0\hat{T}_w$ the temperature of the plates. Then, from assumptions (i) and (ii), the behaviour of the gas is described by the following boundary-value problem for $\hat{f}$:

$$\zeta_1\frac{\partial\hat{f}}{\partial x_1} + \zeta_2\frac{\partial\hat{f}}{\partial x_2} = \frac{1}{k}\hat{Q}(\hat{f}) \quad \left(-\frac{1-\hat{\sigma}}{2} < x_1 < \frac{1-\hat{\sigma}}{2}\right), \tag{2.1a}$$

$$\hat{Q}(\hat{f}) = \frac{1}{2\sqrt{2\pi}}\int\left[\hat{Y}\left(\hat{\rho}\left(x+\frac{1}{2}\hat{\sigma}k\right);\eta_0\right)\hat{f}(x+\hat{\sigma}k,\boldsymbol{\zeta}'_*)\hat{f}(x,\boldsymbol{\zeta}')\right.$$
$$\left. -\hat{Y}\left(\hat{\rho}\left(x-\frac{1}{2}\hat{\sigma}k\right);\eta_0\right)\hat{f}(x-\hat{\sigma}k,\boldsymbol{\zeta}_*)\hat{f}(x,\boldsymbol{\zeta})\right]$$
$$\times(\hat{V}\cdot k)H(\hat{V}\cdot k)\,dk\,d\boldsymbol{\zeta}_*, \tag{2.1b}$$

$$\hat{Y}(\hat{\rho};\eta_0) = \frac{Y(\hat{\rho}\eta_0)}{Y(\eta_0)}, \quad Y(\eta) = \frac{1}{2}\frac{2-\eta}{(1-\eta)^3}, \quad \eta_0 = \frac{(\rho_0/m)\pi\sigma^3}{6}, \tag{2.1c}$$

$$\hat{\rho} = \int\hat{f}\,d\boldsymbol{\zeta}, \tag{2.1d}$$

$$\boldsymbol{\zeta}' = \boldsymbol{\zeta} + (\hat{V}\cdot k)k, \quad \boldsymbol{\zeta}'_* = \boldsymbol{\zeta}_* - (\hat{V}\cdot k)k, \quad \hat{V} = \boldsymbol{\zeta}_* - \boldsymbol{\zeta}, \tag{2.1e}$$

$$k = \frac{\sqrt{\pi}}{2}Kn, \quad Kn = \frac{\ell_0}{D}, \quad \ell_0 = \left[\sqrt{2}\pi\sigma^2(\rho_0/m)Y(\eta_0)\right]^{-1}, \tag{2.1f}$$

$$\text{b.c.:} \quad \hat{f} = \frac{\hat{\rho}_w}{(\pi\hat{T}_w(x_2))^{3/2}}\exp\left(-\frac{\zeta^2}{\hat{T}_w(x_2)}\right) \quad \left(\zeta_1 \gtrless 0, \ x_1 = \mp\frac{1-\hat{\sigma}}{2}\right), \tag{2.1g}$$

$$\hat{\rho}_w = \mp2\sqrt{\frac{\pi}{\hat{T}_w(x_2)}}\int_{\zeta_1\lessgtr0}\zeta_1\hat{f}\,d\boldsymbol{\zeta}, \tag{2.1h}$$

$$\hat{T}_w(x_2) = 1 + c_Tx_2, \tag{2.1i}$$

$$\text{with} \quad \frac{1}{1-\hat{\sigma}}\left.\left(\int_{-(1-\hat{\sigma})/2}^{(1-\hat{\sigma})/2}\int\hat{f}\,d\boldsymbol{\zeta}\,dx_1\right)\right|_{x_2=0} = 1. \tag{2.1j}$$

Here, k is the unit vector in the direction joining the centres of the colliding molecules, H is the Heaviside function, η_0 and $\hat{\rho}\eta_0$ are the volume fractions of molecules corresponding to the average and local densities which indicate denseness of the gas and $\zeta = |\boldsymbol{\zeta}|$, respectively. The quantity ℓ_0 is the mean free path of gas molecules at the equilibrium state at rest with density ρ_0 and temperature T_0. We shall use k in place of the Knudsen number Kn to indicate the degree of gas rarefaction (or smallness of the system). The operator $\hat{Q}$ is the Enskog collision integral, and it includes the parts which are quadratic in $\hat{f}$ like the Boltzmann collision integral. However, colliding molecules occupy different positions due to the finite molecular size, and the collision frequency is increased by the function $\hat{Y}$ that represents an approximate pair correlation function. Hence $\hat{Q}$ is a fivefold integral that is non-local in the position x as well as $\boldsymbol{\zeta}$ and it is more complicated than the Boltzmann collision integral which is local in x. The integration in $\hat{Q}$ is carried out over
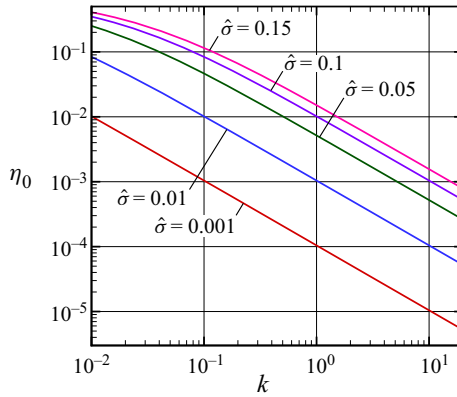
Figure 1. Plot of the volume fraction of molecules η_0 as a function of k for $\hat{\sigma} = 0.001, 0.01, 0.05, 0.1$ and 0.15.

the whole space of $\boldsymbol{\zeta}_*$ and over the whole direction of $\boldsymbol{k}$. In the integral, quantities, here the VDF $\hat{f}(\boldsymbol{x} \pm \hat{\sigma}\boldsymbol{k}, \cdot)$ and the density $\hat{\rho}(\boldsymbol{x} \pm (1/2)\hat{\sigma}\boldsymbol{k})$, are read as zero if their arguments are outside of the domain $\{\boldsymbol{z} = (z_1, z_2, z_3) | |z_1| \leq (1 - \hat{\sigma})/2\}$. This rule is also applied to various integrals appearing later. The functional form (2.1c) of $\hat{Y}$ (or Y) corresponds to the Carnahan–Starling equation of state. The centre of a molecule is able to move in the domain with a width $D - \sigma$, which is narrower than the gap width D by the molecular diameter σ. This fact is reflected in the collision integral (2.1b) and the condition (2.1j) as well as the equation (2.1a) and the boundary condition (2.1g).

Note that the non-dimensional numbers k, $\hat{\sigma}$ and η_0 in (2.1) are not independent but are related as (Sheng *et al.* 2020)

$$k = \frac{\sqrt{\pi}}{2} \hat{\sigma} \frac{1}{6\sqrt{2}\eta_0 Y(\eta_0)}. \tag{2.2}$$

In the present paper, k and $\hat{\sigma}$, the degree of gas rarefaction and the molecular size, are considered as the parameters of the problem. We regard the volume fraction of molecules η_0 as a function of k and $\hat{\sigma}$ determined by (2.2). Its plot is shown in figure 1, which implies that the gas becomes more dense with the decrease of k and the increase of $\hat{\sigma}$ and that it becomes less dense with the increase of k and the decrease of $\hat{\sigma}$.

2.3. *Macroscopic quantities*

For later convenience, here, we introduce the macroscopic variables besides the density given by (2.1d). The flow velocity, temperature, pressure, stress tensor and heat-flow vector are given by $(2RT_0)^{1/2}\hat{v}_i$, $T_0\hat{T}$, $p = p_0\hat{p}$, $p_0\hat{p}_{ij}$ and $p_0(2RT_0)^{1/2}\hat{q}_i$, respectively, where $\hat{v}_i$, $\hat{T}$, $\hat{p}$, $\hat{p}_{ij}$ and $\hat{q}_i$ are defined as the following moments of the VDF $\hat{f}$:

$$\hat{v}_i = \frac{1}{\hat{\rho}} \int \zeta_i \hat{f} \, d\boldsymbol{\zeta}, \tag{2.3a}$$

$$\hat{T} = \frac{2}{3\hat{\rho}} \int (\zeta_k - \hat{v}_k)^2 \hat{f} \, d\boldsymbol{\zeta}, \tag{2.3b}$$

$$\hat{p} = \hat{\rho}\hat{T} \times \frac{1 + \eta + \eta^2 - \eta^3}{(1 - \eta)^3}, \quad \eta = \hat{\rho}\eta_0, \tag{2.3c}$$

962 A20-5

$$\hat{p}_{ij} = \hat{p}_{ij}^{(k)} + \hat{p}_{ij}^{(v)}, \tag{2.3d}$$

$$\hat{p}_{ij}^{(k)} = 2 \int (\zeta_i - \hat{v}_i)(\zeta_j - \hat{v}_j)\hat{f} \, \mathrm{d}\boldsymbol{\zeta}, \tag{2.3e}$$

$$\hat{p}_{ij}^{(v)} = \frac{1}{2\sqrt{2\pi}k} \iint\int_0^{\hat{\sigma}} k_i k_j \hat{Y}\left(\hat{\rho}\left(\boldsymbol{x} + \left(\frac{1}{2}\hat{\sigma} - \hat{\alpha}\right)\boldsymbol{k}\right); \eta_0\right) \hat{f}(\boldsymbol{x} - \hat{\alpha}\boldsymbol{k}, \boldsymbol{\zeta}_*)\hat{f}(\boldsymbol{x} + (\hat{\sigma} - \hat{\alpha})\boldsymbol{k}, \boldsymbol{\zeta})$$
$$\times (\hat{\boldsymbol{V}} \cdot \boldsymbol{k})^2 H(\hat{\boldsymbol{V}} \cdot \boldsymbol{k}) \, \mathrm{d}\hat{\alpha} \, \mathrm{d}\boldsymbol{k} \, \mathrm{d}\boldsymbol{\zeta} \, \mathrm{d}\boldsymbol{\zeta}_*, \tag{2.3f}$$

$$\hat{q}_i = \hat{q}_i^{(k)} + \hat{q}_i^{(v)}, \tag{2.3g}$$

$$\hat{q}_i^{(k)} = \int (\zeta_i - \hat{v}_i)(\zeta_k - \hat{v}_k)^2 \hat{f} \, \mathrm{d}\boldsymbol{\zeta}, \tag{2.3h}$$

$$\hat{q}_i^{(v)} = \frac{1}{4\sqrt{2\pi}k} \iint\int_0^{\hat{\sigma}} k_i \left[(\zeta_\ell' - \hat{v}_\ell)^2 - (\zeta_\ell - \hat{v}_\ell)^2\right]$$
$$\times \hat{Y}\left(\hat{\rho}\left(\boldsymbol{x} + \left(\frac{1}{2}\hat{\sigma} - \hat{\alpha}\right)\boldsymbol{k}\right); \eta_0\right) \hat{f}(\boldsymbol{x} - \hat{\alpha}\boldsymbol{k}, \boldsymbol{\zeta}_*)\hat{f}(\boldsymbol{x} + (\hat{\sigma} - \hat{\alpha})\boldsymbol{k}, \boldsymbol{\zeta})$$
$$\times (\hat{\boldsymbol{V}} \cdot \boldsymbol{k})H(\hat{\boldsymbol{V}} \cdot \boldsymbol{k}) \, \mathrm{d}\hat{\alpha} \, \mathrm{d}\boldsymbol{k} \, \mathrm{d}\boldsymbol{\zeta} \, \mathrm{d}\boldsymbol{\zeta}_*. \tag{2.3i}$$

Equation (2.3c) is the Carnahan–Starling equation of state. The stress tensor $\hat{p}_{ij}$ and the heat-flow vector $\hat{q}_i$ are given by a sum of two parts, respectively. The first part, $\hat{p}_{ij}^{(k)}$ and $\hat{q}_i^{(k)}$, is called the kinetic part and has a familiar form. The second part, $\hat{p}_{ij}^{(v)}$ and $\hat{q}_i^{(v)}$, is called the potential part (Cercignani & Lampis 1988), and it represents the contribution of instantaneous transfers of momentum and energy in binary collisions.

2.4. *Linearization*

Recalling that we consider the situation where the applied temperature and pressure gradients are small (see assumption (iii) in § 2.1), within the linearized regime, we can seek the solution $\hat{f}$ of problem (2.1) as a sum of reference state and perturbation, as follows:

$$\hat{f} = \hat{M}(x_1, \boldsymbol{\zeta}) + \Phi(x_1, x_2, \boldsymbol{\zeta}) + O(\Phi^2) \quad (|\Phi| \ll \hat{M}), \tag{2.4a}$$

$$\hat{M} = \hat{\rho}_M(x_1)E(\zeta), \quad E(\zeta) = \pi^{-3/2}e^{-\zeta^2}, \tag{2.4b}$$

$$\Phi = c_T \left\{ x_2 E(\zeta) \left[\hat{\omega}_T(x_1) + \left(\zeta^2 - \frac{3}{2} \right) \hat{\rho}_M(x_1) \right] + \Psi_T(x_1, \boldsymbol{\zeta}) \right\}$$
$$+ c_P \left[x_2 E(\zeta)\hat{\omega}_P(x_1) + \Psi_P(x_1, \boldsymbol{\zeta}) \right]. \tag{2.4c}$$

Here, some notes may be in order:

(i) The function $\hat{M}$ is the reference state of the gas that is achieved when both the temperature and pressure gradients are absent, i.e. when there is no driving factor in the system. While for an ideal gas (the case of the Boltzmann equation) this state is a uniform equilibrium state at rest, for a dense gas it is an equilibrium state at rest with a density distribution $\hat{\rho}_M(x_1)$ varying in the direction normal to the plates (Frezzotti (1997); see also figure 2(a) shown later). The non-uniformity of the reference density is attributed to the fact that some of intermolecular collisions

which detach the molecules from the plates are forbidden near the boundary due to their finite size and accordingly they are pushed to the plates.

(ii) The function Φ is a perturbation around the reference state $\hat{M}$. In its expression, the subscripts T and P are attached to discriminate the quantities related to the thermal transpiration and Poiseuille flows, respectively. The $O(\Phi^2)$ term in (2.4a) is the negligible error in the linearized regime. As will be seen later in § 4, when the molecular size $\hat{\sigma}$ is finite, the pressure gradient $\partial_{x_2}\hat{p}$ and the stress gradient $\partial_{x_2}\hat{p}_{22}$ are not identical, and moreover they are non-uniform in x_1. Here, the latter is regarded as the driving force for the Poiseuille flow since it is the stress rather than the pressure that has the role of the mechanical surface force. Thus, we require that its average in the x_1 direction be normalized and zero, in accordance with the nature of the Poiseuille and thermal transpiration flows, respectively. To be more precise, with $\hat{p}_{22}$ being evaluated with $\hat{f} = \hat{M} + \Phi$, we require that $(1 - \hat{\sigma})^{-1} \int_{-(1-\hat{\sigma})/2}^{(1-\hat{\sigma})/2} \partial_{x_2}\hat{p}_{22}|_{c_T=0}\, \mathrm{d}x_1 = c_P$ and $(1 - \hat{\sigma})^{-1} \int_{-(1-\hat{\sigma})/2}^{(1-\hat{\sigma})/2} \partial_{x_2}\hat{p}_{22}|_{c_P=0}\, \mathrm{d}x_1 = 0$ for respective flows, where the constant c_P represents the magnitude of the averaged stress gradient in the Poiseuille flow ($|c_P| \ll 1$ by assumption (iii)). Since $\partial_{x_2}\hat{p}_{22} = \partial_{x_2}\hat{p} = \text{const.}$ for the Boltzmann equation, c_P also corresponds to the magnitude of the pressure gradient $(D/p_0)|\,\mathrm{d}p/\mathrm{d}X_2|$ in this case. The parts $c_P x_2 E(\zeta)\hat{\omega}_P(x_1)$ and $c_T x_2 E(\zeta)[\hat{\omega}_T(x_1) + (\zeta^2 - \frac{3}{2})\hat{\rho}_M(x_1)]$ are the perturbed Maxwellians representing the pressure (or stress) and temperature gradients, respectively. Recall that the magnitude of the latter is represented by the coefficient $c_T[= (D/T_0)(\mathrm{d}T_w/\mathrm{d}X_2)]$. The functions Ψ_T and Ψ_P, which are considered to be odd in ζ_2, represent the respective flows.

(iii) The expression (2.4) might look like an arbitrary assumption at a glance, however, it turns out to be an appropriate form of the solution. It is an extension of the similarity solution for a rarefied gas (see also, e.g. (2.8) in Takata & Funagane (2011) or (1) in Ohwada *et al.* 1989) to the case of the dense gas, where the non-uniformity of densities in x_1 is taken into account here due to the finite molecular size both for the reference part $\hat{\rho}_M$ and the perturbed parts $\hat{\omega}_{T,P}$ (the case of Boltzmann equation corresponds to the case $\hat{\rho}_M(x_1) \equiv 1$, $\hat{\omega}_T(x_1) \equiv -1$ and $\hat{\omega}_P(x_1) \equiv 1$). To confirm the consistency of (2.4), actually we can proceed in the following way, which is detailed in Appendix A. First, substitute $\hat{f} = \hat{M} = \hat{\rho}_M E$ into the equation (2.1a) and the condition for average density (2.1j). Then, we reach the system which determines the reference density $\hat{\rho}_M$ (and $\hat{M}$ accordingly) with no inconsistency. Second, introduce the perturbation Φ and substitute $\hat{f} = \hat{M} + \Phi$ (see also (2.4a)) into the equation (2.1a), the boundary condition (2.1g) and the condition for average density (2.1j), and neglect the second- and higher-order terms of perturbation Φ according to assumption (iii). Then, we are left with the linearized system for the perturbation Φ, without any inconsistency. Third, substitute the expression (2.4c) into the system for Φ and closely examine the resulting expressions, in particular those of the collision integral. Then, we find that the form (2.4c) introduces no inconsistency, and the systems for the perturbed densities $\hat{\omega}_{T,P}$ and the VDFs $\Psi_{T,P}$ are accordingly obtained.

2.4.1. *Problems of $\hat{\rho}_M$, $\hat{\omega}_{T,P}$ and $\Psi_{T,P}$*

In (2.4), $\hat{\rho}_M$, $\hat{\omega}_{T,P}$ and $\Psi_{T,P}$ are the functions to be determined. Following the above steps explained in the item (iii) or Appendix A, we find that the densities $\hat{\rho}_M$, $\hat{\omega}_T$ and $\hat{\omega}_P$ satisfy

the following integro-differential equations, while the VDFs Ψ_T and Ψ_P are the solutions of the following boundary-value problems of the linearized Enskog equation:

$$\frac{d\hat{\rho}_M(x_1)}{dx_1} = J_1[\hat{\rho}_M](x_1) \quad \left(-\frac{1-\hat{\sigma}}{2} < x_1 < \frac{1-\hat{\sigma}}{2}\right), \tag{2.5a}$$

$$\text{with} \quad \frac{1}{1-\hat{\sigma}} \int_{-(1-\hat{\sigma})/2}^{(1-\hat{\sigma})/2} \hat{\rho}_M(x_1)\, dx_1 = 1, \tag{2.5b}$$

$$\frac{d\hat{\omega}_\beta(x_1)}{dx_1} = K_1[\hat{\omega}_\beta, \hat{\rho}_M](x_1) \quad \left(-\frac{1-\hat{\sigma}}{2} < x_1 < \frac{1-\hat{\sigma}}{2}\right), \tag{2.6a}$$

$$\text{with} \quad K_2[\hat{\omega}_T, \hat{\rho}_M] = J_2[\hat{\rho}_M] - 1, \tag{2.6b}$$

$$K_2[\hat{\omega}_P, \hat{\rho}_M] = 1, \tag{2.6c}$$

$$\zeta_1 \frac{\partial \Psi_\beta}{\partial x_1} = \frac{1}{k}L(\Psi_\beta) + I_\beta \quad \left(-\frac{1-\hat{\sigma}}{2} < x_1 < \frac{1-\hat{\sigma}}{2}\right), \tag{2.7a}$$

$$\text{b.c.} \quad \Psi_\beta = 0 \quad \left(\zeta_1 \gtrless 0,\ x_1 = \mp\frac{1-\hat{\sigma}}{2}\right). \tag{2.7b}$$

Here, $\beta = T, P$ in (2.6a) and (2.7). The operators J_1, J_2 and J_3 appearing in (2.5a), (2.6b) and the definition (2.11a) of the source term I_T shown later are integrals of $\hat{\rho}_M$ given by (B1) in Appendix B. The operators K_1, K_2 and K_3 appearing in (2.6) and the definition (2.11) of I_β are integrals that are linear with respect to $\hat{\omega}_\beta$ given by (B3) in Appendix B. The integrals J_1 and K_1 represent the contribution coming from the collision integral $\hat{Q}$ to the densities $\hat{\rho}_M$ and $\hat{\omega}_\beta$. Equations (2.6c) and (2.6b) are the reduced form of the aforementioned conditions on the stress gradient $\partial_{x_2}\hat{p}_{22}$ explained in the item (ii) of § 2.4 (see also the last paragraph in Appendix A.3). By these conditions (2.6c) and (2.6b), $\hat{\omega}_P$ and $\hat{\omega}_T$, which satisfy the same linear equation (2.6a) and are thus equal up to a multiplicative constant, are distinguished from each other. The quantity L appearing in (2.7a) is the following Enskog collision operator linearized around the reference local equilibrium state $\hat{M}(x_1, \boldsymbol{\zeta})$:

$$L(\psi)(\boldsymbol{x}, \boldsymbol{\zeta}) = C(\psi)(\boldsymbol{x}, \boldsymbol{\zeta}) - \nu(x_1, \boldsymbol{\zeta})\psi(\boldsymbol{x}, \boldsymbol{\zeta}), \tag{2.8a}$$

$$\begin{aligned}
C(\psi)(\boldsymbol{x}, \boldsymbol{\zeta}) = \frac{1}{2\sqrt{2\pi}} \int \Bigg\{ &\hat{Y}\left(\hat{\rho}_M\left(x_1 + \frac{1}{2}\hat{\sigma}k_1\right); \eta_0\right) \\
&\times \left[\hat{M}(x_1 + \hat{\sigma}k_1, \boldsymbol{\zeta}'_*)\psi(\boldsymbol{x}, \boldsymbol{\zeta}') + \psi(\boldsymbol{x} + \hat{\sigma}\boldsymbol{k}, \boldsymbol{\zeta}'_*)\hat{M}(x_1, \boldsymbol{\zeta}')\right] \\
&- \hat{Y}\left(\hat{\rho}_M\left(x_1 - \frac{1}{2}\hat{\sigma}k_1\right); \eta_0\right)\psi(\boldsymbol{x} - \hat{\sigma}\boldsymbol{k}, \boldsymbol{\zeta}_*)\hat{M}(x_1, \boldsymbol{\zeta}) \\
&+ \hat{Y}_1\left(\hat{\rho}_M\left(x_1 + \frac{\hat{\sigma}}{2}k_1\right); \eta_0\right)\langle\psi\rangle\left(\boldsymbol{x} + \frac{\hat{\sigma}}{2}\boldsymbol{k}\right)\hat{M}(x_1 + \hat{\sigma}k_1, \boldsymbol{\zeta}'_*)\hat{M}(x_1, \boldsymbol{\zeta}') \\
&- \hat{Y}_1\left(\hat{\rho}_M\left(x_1 - \frac{\hat{\sigma}}{2}k_1\right); \eta_0\right)\langle\psi\rangle\left(\boldsymbol{x} - \frac{\hat{\sigma}}{2}\boldsymbol{k}\right)\hat{M}(x_1 - \hat{\sigma}k_1, \boldsymbol{\zeta}_*)\hat{M}(x_1, \boldsymbol{\zeta}) \Bigg] \Bigg\} \\
&\times (\hat{\boldsymbol{V}} \cdot \boldsymbol{k})H(\hat{\boldsymbol{V}} \cdot \boldsymbol{k})\, d\boldsymbol{k}\, d\boldsymbol{\zeta}_*,
\end{aligned} \tag{2.8b}$$

$$v(x_1, \zeta) = \frac{1}{2\sqrt{2\pi}} \int \hat{Y}\left(\hat{\rho}_M\left(x_1 - \frac{1}{2}\hat{\sigma}k_1\right); \eta_0\right)$$
$$\times \hat{M}(x_1 - \hat{\sigma}k_1, \zeta_*)(\hat{V} \cdot k)H(\hat{V} \cdot k) \, dk \, d\zeta_*, \tag{2.8c}$$

where

$$\hat{Y}_1(r; \eta_0) = \frac{1}{Y(\eta_0)} \frac{\eta_0(5 - 2r\eta_0)}{2(1 - r\eta_0)^4}, \tag{2.9a}$$

$$\langle \psi \rangle (x) = \int \psi(x, \zeta) \, d\zeta. \tag{2.9b}$$

In the decomposition (2.8a) of L, C is the integral operator with some smoothing property in the molecular velocity ζ and v is the collision frequency for the reference equilibrium state $\hat{M}(x_1, \zeta)$. The function $\hat{Y}_1$ given in (2.9a) is just a perturbed part of $\hat{Y}$ such that

$$\hat{Y}(\hat{\rho}_M + c \langle \psi \rangle; \eta_0) = \hat{Y}(\hat{\rho}_M; \eta_0) + c \langle \psi \rangle \hat{Y}_1(\hat{\rho}_M; \eta_0) + O(c^2) \ (|c| \ll 1). \tag{2.10}$$

The source term I_β in (2.7a) is given in terms of the densities $\hat{\rho}_M$ and $\hat{\omega}_{T,P}$ as

$$I_T(x_1, \zeta) = -\zeta_2 E(\zeta)\left[\hat{\rho}_M(x_1)\left(\zeta^2 - \frac{3}{2}\right) + \hat{\omega}_T(x_1)\right]$$
$$- \frac{\hat{\sigma}E(\zeta)}{k2\sqrt{2\pi}}\left\{\zeta_2 K_3[\hat{\omega}_T, \hat{\rho}_M](x_1) + J_3[\hat{\rho}_M](x_1, \zeta)\right\}, \tag{2.11a}$$

$$I_P(x_1, \zeta) = -\zeta_2 E(\zeta)\hat{\omega}_P(x_1) - \frac{\hat{\sigma}}{k2\sqrt{2\pi}}\zeta_2 E(\zeta)K_3[\hat{\omega}_P, \hat{\rho}_M](x_1). \tag{2.11b}$$

Thanks to the symmetry of the present problem with respect to the middle of the gap $x_1 = 0$, we can seek the VDF Ψ_β with the following property:

$$\Psi_\beta(x_1, \zeta_1, \zeta_2, \zeta_3) = \Psi_\beta(-x_1, -\zeta_1, \zeta_2, \zeta_3) \quad \left(0 < x_1 < \frac{1 - \hat{\sigma}}{2}; \beta = T, P\right). \tag{2.12}$$

Thus, hereafter, we impose the following condition:

$$\Psi_\beta(0, \zeta_1, \zeta_2, \zeta_3) = \Psi_\beta(0, -\zeta_1, \zeta_2, \zeta_3) \tag{2.13}$$

on Ψ_β, which is obtained by substituting $x_1 = 0$ into (2.12), and we consider the problem of Ψ_β on $-(1 - \hat{\sigma})/2 < x_1 < 0$.

2.4.2. *Expressions of macroscopic quantities*
Substituting the solution (2.4) into (2.1d), (2.3a)–(2.3c), (2.3e), (2.3f), (2.3h) and (2.3i), within negligible error $O(c_P^2, c_T^2)$ in the linearized regime, we have the following expressions for the macroscopic quantities $\hat{\rho}$, $\hat{v}_i$, $\hat{T}$, $\hat{p}$, $\hat{p}_{ij}^{(k)}$, $\hat{p}_{ij}^{(v)}$, $\hat{q}_i^{(k)}$ and $\hat{q}_i^{(v)}$:

$$\hat{\rho} = \hat{\rho}_M(x_1) + c_T x_2 \hat{\omega}_T(x_1) + c_P x_2 \hat{\omega}_P(x_1) + O(c_P^2, c_T^2), \tag{2.14a}$$

$$\hat{v}_2 = c_T u[\Psi_T](x_1) + c_P u[\Psi_P](x_1) + O(c_P^2, c_T^2), \tag{2.14b}$$

$$\hat{v}_1 = O(c_P^2, c_T^2), \quad \hat{v}_3 = O(c_P^2, c_T^2), \tag{2.14c}$$

$$\hat{T} = 1 + c_T x_2 + O(c_P^2, c_T^2), \tag{2.14d}$$

$$\hat{p} = \hat{\rho}_M(x_1)S_1(\hat{\rho}_M(x_1)\eta_0) + c_T x_2 G_T(x_1) + c_P x_2 G_P(x_1) + O(c_P^2, c_T^2), \qquad (2.14e)$$

$$\hat{p}_{22}^{(k)} = \hat{\rho}_M(x_1) + c_T x_2 G_{22,T}^{(k)}(x_1) + c_P x_2 G_{22,P}^{(k)}(x_1) + O(c_P^2, c_T^2), \qquad (2.14f)$$

$$\hat{p}_{12}^{(k)} = c_T P_{12}^{(k)}[\Psi_T](x_1) + c_P P_{12}^{(k)}[\Psi_P](x_1) + O(c_P^2, c_T^2), \qquad (2.14g)$$

$$\hat{p}_{11}^{(k)} = \hat{p}_{22}^{(k)} + O(c_P^2, c_T^2), \quad \hat{p}_{33}^{(k)} = \hat{p}_{22}^{(k)} + O(c_P^2, c_T^2),$$

$$\hat{p}_{13}^{(k)} = O(c_P^2, c_T^2), \quad \hat{p}_{23}^{(k)} = O(c_P^2, c_T^2), \qquad (2.14h)$$

$$\hat{p}_{11}^{(v)} = P_{11,M}^{(v)}(x_1) + c_T x_2 G_{11,T}^{(v)}(x_1) + c_P x_2 G_{11,P}^{(v)}(x_1) + O(c_P^2, c_T^2), \qquad (2.14i)$$

$$\hat{p}_{22}^{(v)} = P_{22,M}^{(v)}(x_1) + c_T x_2 G_{22,T}^{(v)}(x_1) + c_P x_2 G_{22,P}^{(v)}(x_1) + O(c_P^2, c_T^2), \qquad (2.14j)$$

$$\hat{p}_{12}^{(v)} = c_T P_{12,T}^{(v)}(x_1) + c_P P_{12,P}^{(v)}(x_1) + O(c_P^2, c_T^2), \qquad (2.14k)$$

$$\hat{p}_{33}^{(v)} = \hat{p}_{22}^{(v)} + O(c_P^2, c_T^2), \quad \hat{p}_{13}^{(v)} = O(c_P^2, c_T^2), \quad \hat{p}_{23}^{(v)} = O(c_P^2, c_T^2), \qquad (2.14l)$$

$$\hat{q}_2^{(k)} = c_T Q^{(k)}[\Psi_T](x_1) + c_P Q^{(k)}[\Psi_P](x_1) + O(c_P^2, c_T^2), \qquad (2.14m)$$

$$\hat{q}_2^{(v)} = c_T Q_T^{(v)}(x_1) + c_P Q_P^{(v)}(x_1) + O(c_P^2, c_T^2), \qquad (2.14n)$$

$$\hat{q}_1^{(k)} = O(c_P^2, c_T^2), \quad \hat{q}_3^{(k)} = O(c_P^2, c_T^2), \quad \hat{q}_1^{(v)} = O(c_P^2, c_T^2), \quad \hat{q}_3^{(v)} = O(c_P^2, c_T^2). \qquad (2.14o)$$

Here,

$$u[\Psi_\beta] = \frac{1}{\hat{\rho}_M} \int \zeta_2 \Psi_\beta \, \mathrm{d}\boldsymbol{\zeta}, \qquad (2.15a)$$

$$G_T = \hat{\rho}_M(x_1)S_1(\hat{\rho}_M(x_1)\eta_0) + \hat{\omega}_T(x_1)[S_1(\hat{\rho}_M(x_1)\eta_0) + S_2(\hat{\rho}_M(x_1)\eta_0)], \qquad (2.15b)$$

$$G_P = \hat{\omega}_P(x_1)[S_1(\hat{\rho}_M(x_1)\eta_0) + S_2(\hat{\rho}_M(x_1)\eta_0)], \qquad (2.15c)$$

$$S_1(r) = \frac{1 + r + r^2 - r^3}{(1-r)^3}, \quad S_2(r) = \frac{2r(2 + 2r - r^2)}{(1-r)^4}, \qquad (2.15d)$$

$$G_{22,T}^{(k)} = \hat{\rho}_M(x_1) + \hat{\omega}_T(x_1), \quad G_{22,P}^{(k)} = \hat{\omega}_P(x_1), \qquad (2.15e)$$

$$P_{12}^{(k)}[\Psi_\beta] = 2 \int \zeta_1 \zeta_2 \Psi_\beta \, \mathrm{d}\boldsymbol{\zeta}, \qquad (2.15f)$$

$$P_{12,\beta}^{(v)}(x_1) = P_{12,\omega_\beta}^{(v)}(x_1) + P_{12}^{(v)}[\Psi_\beta](x_1), \qquad (2.15g)$$

$$Q^{(k)}[\Psi_\beta] = \int \zeta_2 \left(\zeta^2 - \frac{5}{2}\right) \Psi_\beta \, \mathrm{d}\boldsymbol{\zeta}, \qquad (2.15h)$$

$$Q_T^{(v)} = Q^{(v)}[\Psi_T](x_1) - \left\{ u[\Psi_T](x_1) + \frac{\hat{\sigma}}{\sqrt{2\pi}} \right\} P_{22,M}^{(v)}(x_1), \qquad (2.15i)$$

$$Q_P^{(v)} = Q^{(v)}[\Psi_P](x_1) - u[\Psi_P](x_1) P_{22,M}^{(v)}(x_1). \qquad (2.15j)$$

The expressions of the stress contributions $P_{11,M}^{(v)}$, $P_{22,M}^{(v)}$, $P_{12,\omega_T}^{(v)}$ and $P_{12,\omega_P}^{(v)}$ and the gradients $G_{11,T}^{(v)}$, $G_{11,P}^{(v)}$, $G_{22,T}^{(v)}$ and $G_{22,P}^{(v)}$, which are all defined as the integrals of the densities $\hat{\rho}_M$, $\hat{\omega}_T$ and $\hat{\omega}_P$, and those of $P_{12}^{(v)}[\Psi_\beta]$ and $Q^{(v)}[\Psi_\beta]$, are given in Appendix C. Note that $c_T G_T$, $c_T(G_{22,T}^{(k)} + G_{22,T}^{(v)})$ and $c_T(Q^{(k)}[\Psi_T] + Q_T^{(v)})$ (or $c_P G_P$, $c_P(G_{22,P}^{(k)} + G_{22,P}^{(v)})$

962 A20-10

and $c_P(Q^{(k)}[\Psi_P] + Q_P^{(v)}))$ are the gradient of pressure $\partial_{x_2}\hat{p}$, that of the $(2, 2)$ component of stress $\partial_{x_2}\hat{p}_{22}$ and the heat flow $\hat{q}_2$ for the thermal transpiration (or Poiseuille) flow, respectively, within the linearized regime (see (2.14*e*), (2.3*d*), (2.14*f*), (2.14*j*), (2.3*g*), (2.14*m*) and (2.14*n*)).

It is better to mention again the expression (2.14) is obtained within the linearized regime. At a glance, it might look strange that the temperature $\hat{T}$ is uniform for the Poiseuille flow and that the diagonal kinetic-part stress components are equal to each other (see (2.14*d*) with $c_T = 0$ and (2.14*h*)). However, they are justified in the linearized regime, and deviations from them are attributed to nonlinear effects of $O(c_P^2, c_T^2)$, which are neglected here due to the smallness (see also the last sentence in § 2.1). The coefficients $c_{P,T}$ need to be sufficiently small compared with 1, and, in addition, compared with the degree of gas rarefaction k when we consider the flow with small k. (Some of the quantities of interest in the present paper are of $O(k)$ rather than $O(1)$.) Although there is no definite threshold, e.g. when $c_{P,T} \lesssim 0.001$ or $c_{P,T} \lesssim 0.0001$, the nonlinear effects would likely not be significant for the cases presented in § 4, where k is in the range [0.05, 10].

Also, as in other works based on the linearization assumption, flows between two infinitely wide parallel plates are considered in the present work. Thus, when flow in a finite-length channel with moderate pressure and temperature differences is considered, its length (and the lateral width when a rectangular channel is considered as in experiments) needs to be sufficiently long compared with both its gap width D and the mean free path so that the results for infinitely wide plates give a good description of the flow (Sharipov 1999). Note that, for the case of a rarefied gas, there is an experiment of pressure-driven flow (Ewart *et al.* 2007) taking this condition carefully into consideration (the channel length and lateral width are respectively approximately 1000 and 52 times the gap width). There, it is reported that the experimental results agree well with numerical results for infinitely wide plates (Loyalka 1975) based on a model kinetic equation for a wide range of the Knudsen number approximately up to 10.

2.4.3. *Net mass flow and conservation law*

Denoting by $\rho_0(2RT_0)^{1/2}D\mathcal{M}$ the net mass flow through the gap per unit time and unit length in X_3, $\mathcal{M}$ is given as

$$\mathcal{M} = c_T\mathcal{M}_T + c_P\mathcal{M}_P + O(c_P^2, c_T^2), \tag{2.16}$$

where

$$\mathcal{M}_\beta = \int_{-(1-\hat{\sigma})/2}^{(1-\hat{\sigma})/2} \hat{\rho}_M(s)u[\Psi_\beta](s)\,\mathrm{d}s. \tag{2.17}$$

Multiplying (2.1*a*) by ζ_2 and integrating the result over the whole space of $\boldsymbol{\zeta}$, we have the following conservation equation for the momentum in the x_2 direction within negligible error in the linearized regime:

$$\frac{\partial\hat{p}_{12}}{\partial x_1} + \frac{\partial\hat{p}_{22}}{\partial x_2} = O(c_P^2, c_T^2). \tag{2.18}$$

Substituting the expression of $\hat{p}_{12}$ and $\hat{p}_{22}$ (see (2.3*d*), (2.14*f*), (2.14*g*), (2.14*j*) and (2.14*k*)) into (2.18) and integrating the result over $[-(1 - \hat{\sigma})/2, x_1]$ with respect to x_1, we obtain

$$c_T S_T(x_1) + c_P S_P(x_1) = O(c_P^2, c_T^2), \tag{2.19}$$

where

$$S_\beta(x_1) = P_{12}^{(k)}[\Psi_\beta](x_1) + P_{12,\beta}^{(v)}(x_1) - P_{12}^{(k)}[\Psi_\beta]\left(-\frac{1-\hat\sigma}{2}\right)$$
$$+ \int_{-(1-\hat\sigma)/2}^{x_1}\left[G_{22,\beta}^{(k)}(s) + G_{22,\beta}^{(v)}(s)\right]\mathrm{d}s. \tag{2.20}$$

In obtaining (2.20), we have used the fact that the potential part of the stress $P_{12,\beta}^{(v)}$ vanishes on the boundary $x_1 = -(1-\hat\sigma)/2$. The relation (2.19) will be used for the accuracy test of our computation.

3. Numerical method

The densities $\hat\rho_M$, $\hat\omega_T$ and $\hat\omega_P$, which are defined by (2.5) and (2.6), can be obtained numerically by the method in Frezzotti (1997). Thus, the problem is reduced to (2.7) with (2.13) for the VDFs Ψ_T and Ψ_P.

Let us explain the numerical solution method for the problems of Ψ_T and Ψ_P. We solve them by using iteration based on the integral formulation (Takata & Funagane 2011; Hattori & Takata 2015) of the Enskog equation combined with the fast Fourier spectral method (Filbet *et al.* 2006) for the computation of the collision integral. Taking into account (2.8a) and (2.13) and formally integrating the equation (2.7a) with respect to x_1, we have

$$\Psi_\beta(x_1,\boldsymbol\zeta) = \int_{-(1-\hat\sigma)/2}^{x_1}\left[\frac{1}{k\zeta_1}C(\Psi_\beta)(s,\boldsymbol\zeta) + \frac{1}{\zeta_1}I_\beta(s,\boldsymbol\zeta)\right]\exp\left(-\frac{1}{k\zeta_1}\int_s^{x_1}\nu(p,\boldsymbol\zeta)\,\mathrm{d}p\right)\mathrm{d}s,$$
$$\left(-\frac{1-\hat\sigma}{2} < x_1 < 0,\ \zeta_1 > 0\right), \tag{3.1a}$$

$$\Psi_\beta(x_1,\boldsymbol\zeta) = \Psi_\beta(0,\boldsymbol\zeta^-)\exp\left(-\frac{1}{k\zeta_1}\int_0^{x_1}\nu(p,\boldsymbol\zeta)\,\mathrm{d}p\right)$$
$$+ \int_0^{x_1}\left[\frac{1}{k\zeta_1}C(\Psi_\beta)(s,\boldsymbol\zeta) + \frac{1}{\zeta_1}I_\beta(s,\boldsymbol\zeta)\right]\exp\left(-\frac{1}{k\zeta_1}\int_s^{x_1}\nu(p,\boldsymbol\zeta)\,\mathrm{d}p\right)\mathrm{d}s,$$
$$\left(-\frac{1-\hat\sigma}{2} < x_1 < 0,\ \zeta_1 < 0\right), \tag{3.1b}$$

where $\boldsymbol\zeta^- = (-\zeta_1,\zeta_2,\zeta_3)$ and $\beta = T, P$. Since C is an integral operator, $C(\Psi_\beta)$ is mild in $\boldsymbol\zeta$ even if its argument function Ψ_β is not. Thus, the factor of steep variation of Ψ_β in $\boldsymbol\zeta$ (or ζ_1) is explicit in this formulation, which will be advantageous in accurately capturing the structure of the solution. The solution Ψ_β is constructed by iteration based on (3.1) from its initial guess. The data of $C(\Psi_\beta)$ are computed by the fast Fourier spectral method from the given data of Ψ_β. The fast Fourier spectral method for the nonlinear Enskog collision integral is explained in Wu *et al.* (2015). Following the reference, we can prepare the method for the linearized Enskog collision operator C in the present work. The spatial integration with respect to p and that with respect to s in (3.1) are performed analytically after ν and $(C(\Psi_\beta), I_\beta)$ are interpolated respectively with piecewise linear and quadratic functions from their data on the lattice points for position x_1.

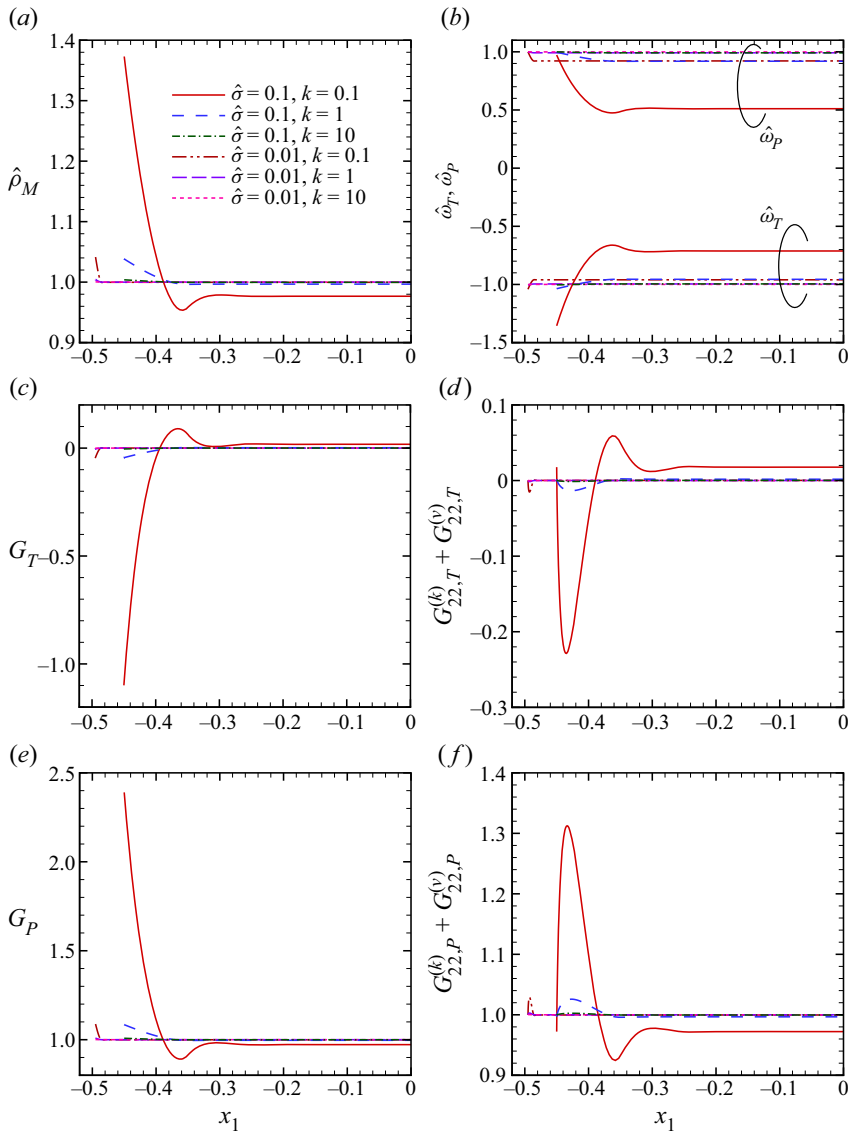Information of lattice systems and accuracy is briefly given in Appendix D.

Figure 2. Profiles of quantities related to the density and the gradients of the pressure and the $(2, 2)$ component of stress; (a) $\hat{\rho}_M$, (b) $\hat{\omega}_T$ and $\hat{\omega}_P$, (c) G_T, (d) $G_{22,T}^{(k)} + G_{22,T}^{(v)}$, (e) G_P and (f) $G_{22,P}^{(k)} + G_{22,P}^{(v)}$.

4. Numerical results and discussions

Figure 2 shows the quantities related to the density and the gradients of the pressure and the $(2, 2)$ component of stress in the x_2-direction, namely $\hat{\rho}_M$, $\hat{\omega}_T$ and $\hat{\omega}_P$, G_T, $G_{22,T}^{(k)} + G_{22,T}^{(v)}$, G_P and $G_{22,P}^{(k)} + G_{22,P}^{(v)}$, for the molecular-size parameter $\hat{\sigma} = 0.01$ and 0.1 and the degree of gas rarefaction $k = 0.1$, 1 and 10 (see also the last sentence of the first paragraph in § 2.4.2). The profiles for small $\hat{\sigma}$ and large k (e.g. for $\hat{\sigma} = 0.01$ and $k = 10$) are almost uniform and close to their counterparts for the Boltzmann equation. On the other hand, for large $\hat{\sigma}$ and small k (e.g. for $\hat{\sigma} = 0.1$ and $k = 0.1$), or when the gas is dense, they vary significantly near the boundary and are non-uniform in the x_1 direction. As for the

962 A20-13

origin of the non-uniformity of densities $\hat{\rho}_M$ and $\hat{\omega}_{T,P}$ (figure 2*a,b*), see also the item (i) in § 2.4. The gradient of the pressure actually differs from that of the (2, 2) component of stress (compare figures 2*c* and 2*d*, and figures 2*e* and 2*f*), even if their averages over x_1 are taken. This is in marked contrast to the case of an ideal gas (or the Boltzmann equation), in which the gradients of the pressure and the normal stress components are uniform and identical for each of the two flows considered here. The stress gradient for the thermal transpiration flow is negative near the boundary and positive in the central part of the gap (figure 2*d*). That for the Poiseuille flow is smaller in the central part of the gap than near the boundary (figure 2*f*).

The densities $\hat{\rho}_M(x_1)$ and $\hat{\omega}_P(x_1)$ shown in figure 2 seem to vary significantly only near the boundary within the distance $O(\hat{\sigma})$ and approach their values $\hat{\rho}_M(0)$ and $\hat{\omega}_P(0)$ at the middle of the gap. By using the rescaled distance from the boundary $(x_1 + (1 - \hat{\sigma})/2)/\hat{\sigma}$ and semilog plot, figure 3(*a–d*) demonstrates this observation. The approach to the values $\hat{\rho}_M(0)$ and $\hat{\omega}_P(0)$ in the uniform region is actually sufficiently fast in the scale of $O(\hat{\sigma})$. Moreover, the magnitude of the deviation between the density on the boundary and that at the middle of the gap is of the order of the volume fraction of molecules η_0 (figure 3*e,f*). From these results, when $\hat{\sigma}$ and k are decreased simultaneously so that η_0 is finite, a thin layer with the thickness of $O(\hat{\sigma})$ adjacent to the boundary, where the densities deviate up to $O(\eta_0)$ from their values in the uniform region outside the layer, is expected to appear.

In figure 4, the profiles of the mass flow $\hat{\rho}_M u[\Psi_T]$ for the thermal transpiration flow are shown for various values of the degree of gas rarefaction k and the molecular-size parameter $\hat{\sigma}$. When k is not small, the flow is smaller for larger $\hat{\sigma}$ (see panel *a*). Its main reason is simply that the increase of the temperature along the plate in units of the effective width $D - \sigma$ where the centre of a molecule can move, which becomes shorter for larger σ, is small, so that the flow is less driven. This effect is more significant than the enhancement of the flow due to the increase of the effective Knudsen number defined with the length $D - \sigma$, which should be taken into account too. Related observation will be done for the net mass flow shown later. When k is relatively small, in turn, as $\hat{\sigma}$ increases, the flow is enhanced over the whole gap including near the boundary. Indeed, for $k = 0.1$, the mass flow is larger for larger $\hat{\sigma}$ (see panel *b*). This is expected to be associated with the increase of the thermal conductivity of the gas accompanied by the increase of $\hat{\sigma}$, which is explained by the Chapman–Enskog theory for a dense gas (Chapman & Cowling 1991) for small Knudsen numbers, because the thermal slip coefficient, which approximately represents the magnitude of the induced flow, is likely larger for the gas with larger thermal conductivity, judging from the relation between them for monoatomic rarefied gases. The negative gradient of stress near the boundary also contributes to the increase of the mass flow there (see figure 2*d*). With further decrease of k, we observe considerable decrease of the mass flow in the central part of the gap (see figure 4*c,d*). Figure 2(*d*) implies that this is due to the deceleration by the positive gradient of stress there. Incidentally, when k is small and $\hat{\sigma}$ is large, although the profile of the flow velocity $u[\Psi_T]$ differs quantitatively from the mass flow $\hat{\rho}_M u[\Psi_T]$ due to the non-uniformity of $\hat{\rho}_M$, the qualitative features mentioned above are in common with $u[\Psi_T]$.

The profiles of the mass flow $\hat{\rho}_M u[\Psi_P]$ for the Poiseuille flow are shown in figure 5 for various values of the degree of gas rarefaction k and the molecular-size parameter $\hat{\sigma}$. The profile is flatter and the flow is smaller for larger $\hat{\sigma}$, which is consistent with the fact that the magnitude of the Poiseuille flow is roughly inversely proportional to the viscosity for small k and its increase is accompanied by the increase of $\hat{\sigma}$.

Figure 6 shows the profiles of the heat flow for the thermal transpiration flow. When k is small, the heat flow is enhanced for larger $\hat{\sigma}$, which is consistent with the aforementioned
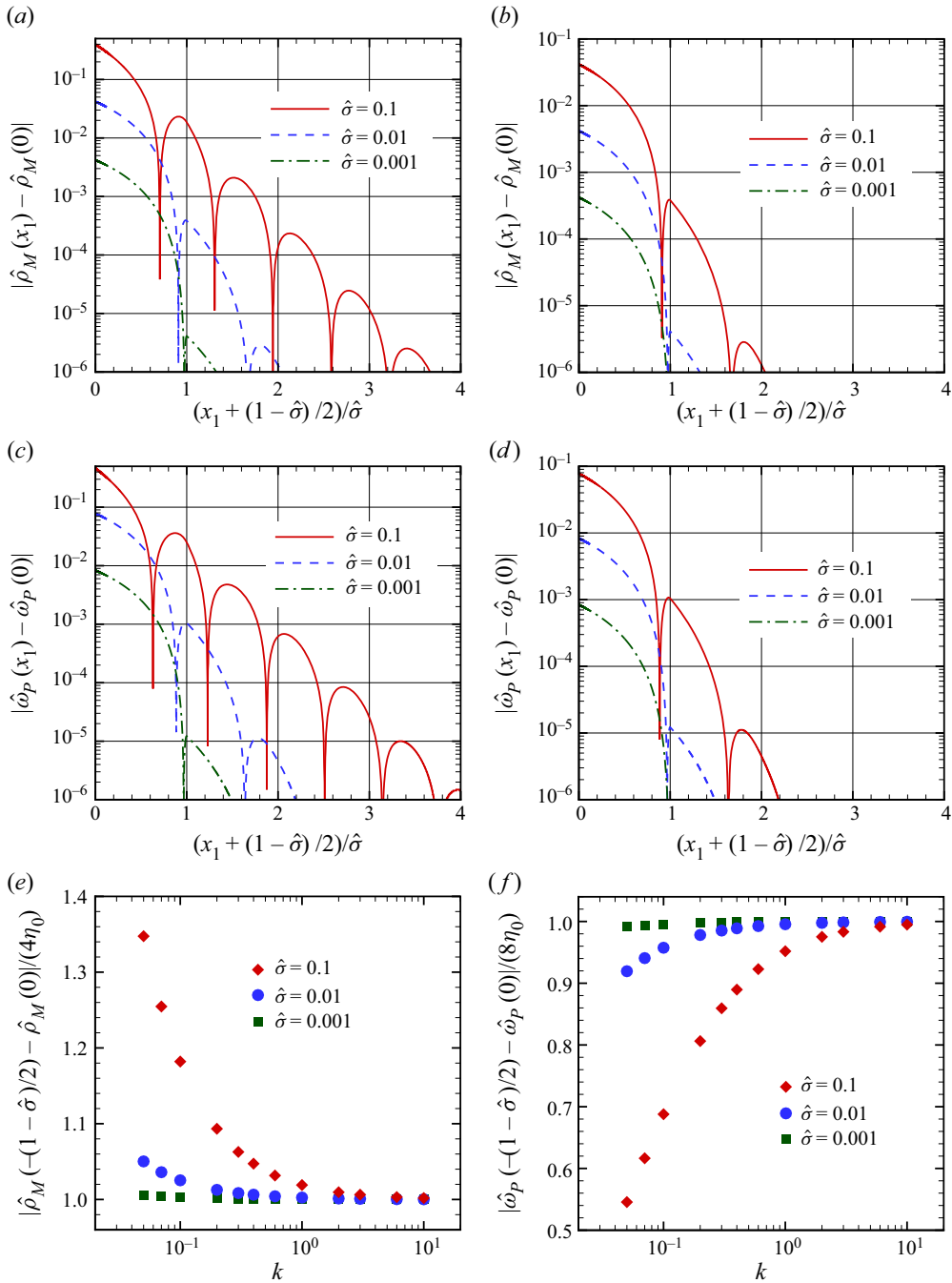
Figure 3. Deviation of densities $\hat{\rho}_M$ and $\hat{\omega}_P$ from their values at the middle of the gap; (a) $|\hat{\rho}_M(x_1) - \hat{\rho}_M(0)|$ for $k = 0.1$, (b) $|\hat{\rho}_M(x_1) - \hat{\rho}_M(0)|$ for $k = 1$, (c) $|\hat{\omega}_P(x_1) - \hat{\omega}_P(0)|$ for $k = 0.1$, (d) $|\hat{\omega}_P(x_1) - \hat{\omega}_P(0)|$ for $k = 1$, (e) $|\hat{\rho}_M(-(1-\hat{\sigma})/2) - \hat{\rho}_M(0)|/(4\eta_0)$ and (f) $|\hat{\omega}_P(-(1-\hat{\sigma})/2) - \hat{\omega}_P(0)|/(8\eta_0)$. In (a–d), the quantities are plotted as functions of $(x_1 + (1-\hat{\sigma})/2)/\hat{\sigma}$, the distance from the boundary scaled by the molecular diameter $\hat{\sigma}$. In (e,f), the quantities are scaled by the volume fraction of molecules η_0 and plotted as functions of k.
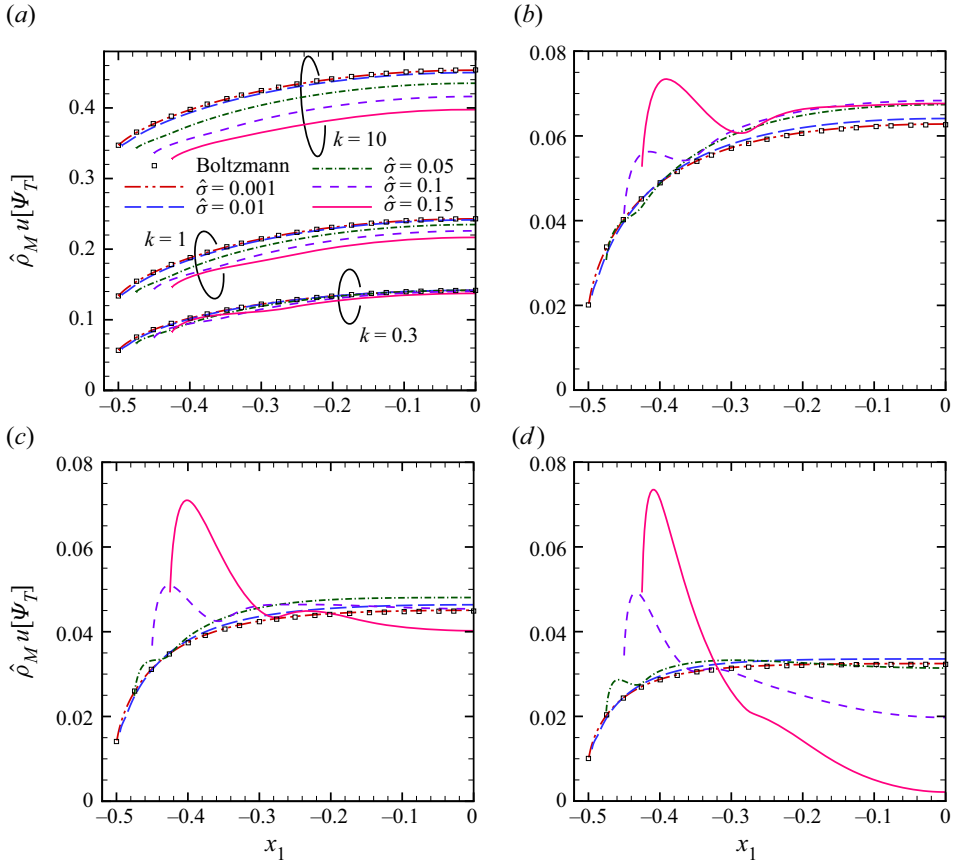
Figure 4. Profiles of the mass flow of the thermal transpiration flow; $\hat{\rho}_M u[\Psi_T]$ vs x_1. (a) $k = 10$, 1 and 0.3, (b) $k = 0.1$, (c) $k = 0.07$ and (d) $k = 0.05$.

increase of the thermal conductivity. It changes steeply near the boundary for large $\hat{\sigma}$ as in the mass flow. The profile of the heat flow for the Poiseuille flow is shown in figure 7. This heat flow is known to be owing to the effect of gas rarefaction in the case of an ideal gas since it occurs under the isothermal condition and it has no direct relation to the thermal conductivity and viscosity. Our result shows that heat flow of this kind is also enhanced with the increase of $\hat{\sigma}$.

Let us consider the force-driven flow, a flow driven by a uniform external force in the direction parallel to the plates. This flow has been studied in the framework of kinetic theory with an interest in non-Navier–Stokes effects such as the heat flow along the force direction, the temperature bimodality and the anisotropy of normal stress components (see, e.g. Tij & Santos 1994; Malek Mansour, Baras & Garcia 1997). Note that these are nonlinear effects, i.e. they manifest themselves at second order in the magnitude of the normalized force. The behaviour of the mass flow of the Poiseuille flow observed in figure 5 is similar to that of the force-driven flow within the linearized regime for small force (Wu *et al.* 2016; Sheng *et al.* 2020), where the aforementioned effects are suppressed sufficiently. Thus, we have also carried out the computations of the latter case, which is described by the solution of the problem (2.7) of Ψ_P with the source term I_P being replaced
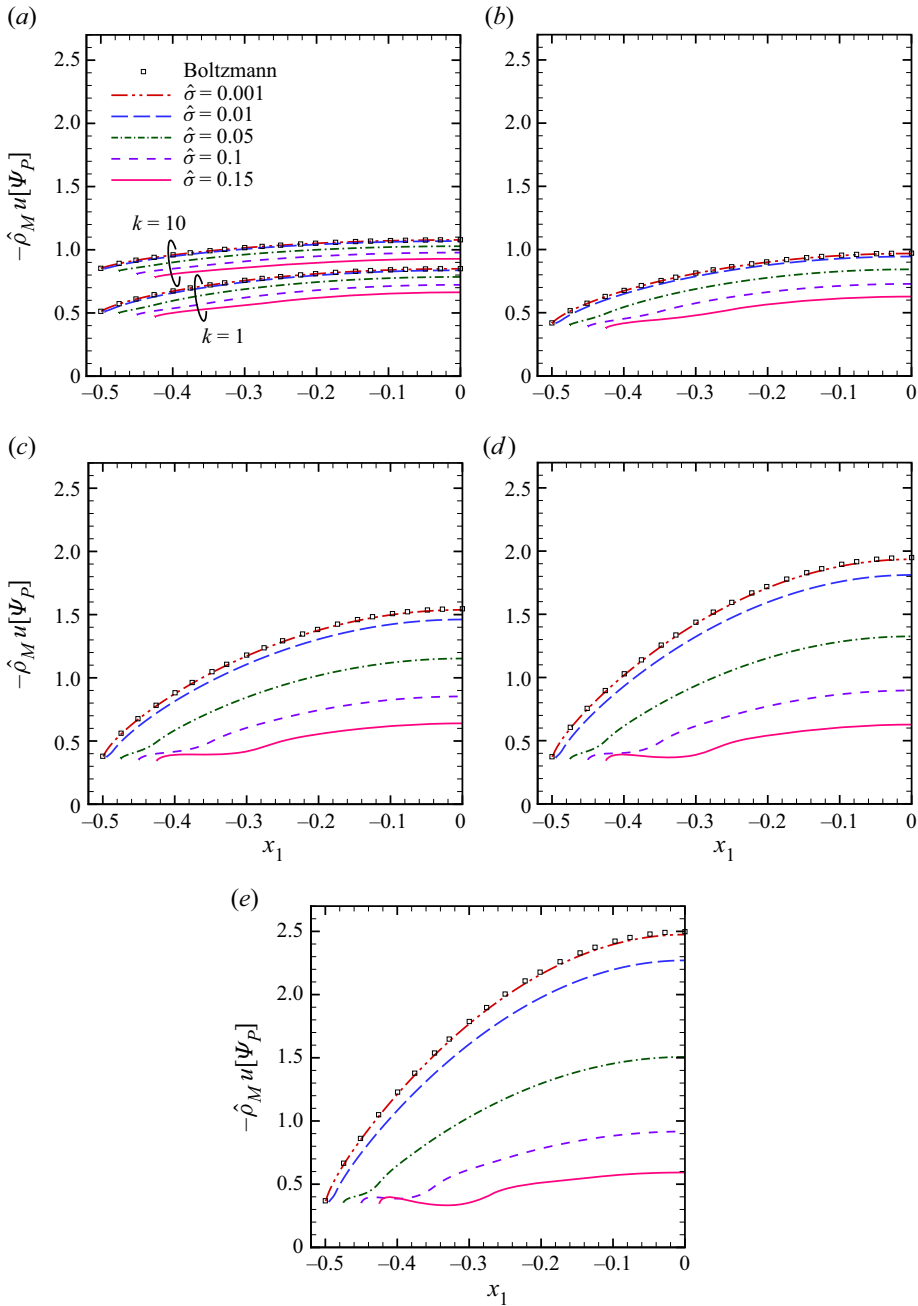
962 A20-16

Figure 5. Profiles of the mass flow of the Poiseuille flow; $\hat{\rho}_M u[\Psi_P]$ vs x_1. (*a*) $k = 10$ and 1, (*b*) $k = 0.3$, (*c*) $k = 0.1$, (*d*) $k = 0.07$ and (*e*) $k = 0.05$.

by

$$- \zeta_2 \hat{\rho}_M E \equiv I_F. \tag{4.1}$$

Since I_P and I_F are identical for the Boltzmann equation (both are given by $-\zeta_2 E$), so are the VDFs (Ψ_P and its counterpart) and the flow velocities, heat flows and shear stresses obtained as their moments. On the other hand, for the case of a dense gas, there
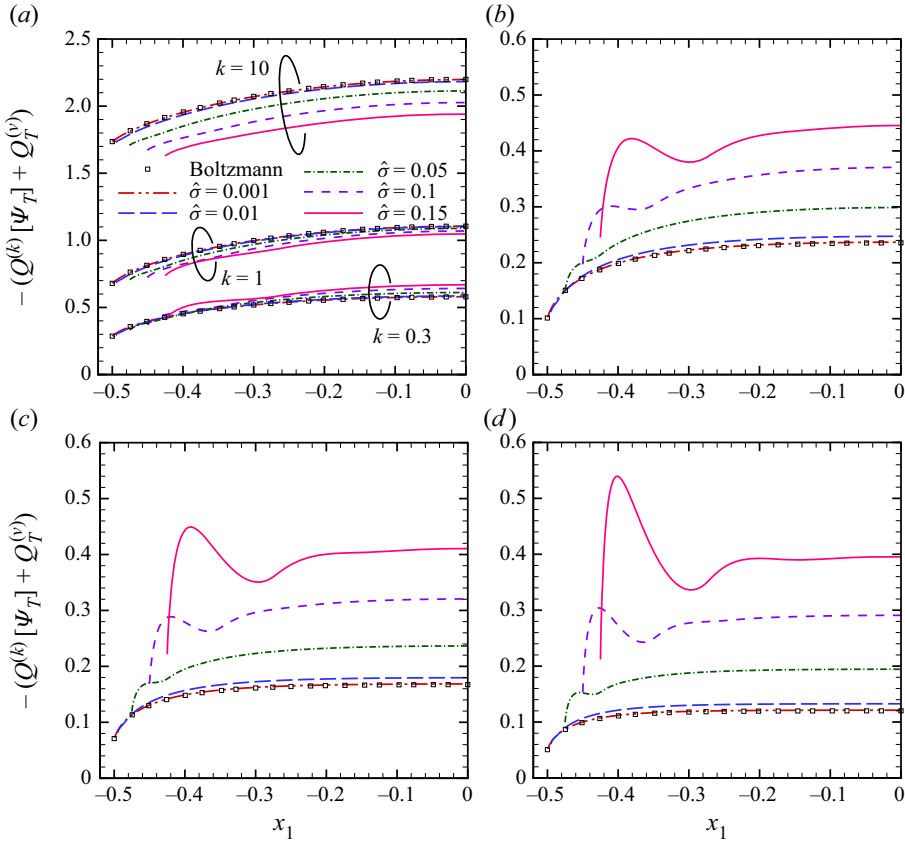
Figure 6. Profiles of the heat flow of the thermal transpiration flow; $Q^{(k)}[\Psi_T] + Q_T^{(v)}$ vs x_1; (a) $k = 10$, 1 and 0.3, (b) $k = 0.1$, (c) $k = 0.07$ and (d) $k = 0.05$.

are differences for the profiles of mass and heat flows between two cases although the differences are very slight (see figure 8(a,b), in particular, the curves for $\hat{\sigma} = 0.15$). Recall that the expressions of I_P and I_F (see (2.11b) and (4.1)) differ for the case of a dense gas. Actually, there is a difference between their marginal functions

$$\int_{-\infty}^{\infty} \int_0^{\infty} (I_P(x_1, \boldsymbol{\zeta}), I_F(x_1, \boldsymbol{\zeta})) \, \mathrm{d}\zeta_2 \, \mathrm{d}\zeta_3 \equiv (I_P^{\dagger}(x_1, \zeta_1), I_F^{\dagger}(x_1, \zeta_1)) \tag{4.2}$$

near the boundary for large $\hat{\sigma}$, as shown in figure 8(c,d). For $\hat{\sigma} = 0.1$ and $x_1 = -0.45$, their difference normalized by the maximum, $\max_{\zeta_1} |I_P^{\dagger} - I_F^{\dagger}| / \max_{\zeta_1} |I_F^{\dagger}|$, is larger than 0.051 (5.1 %). This demonstrates that, for the case of the Enskog equation, there are differences between the force-driven and the pressure-driven flows even within the linearized regime, especially at the microscopic level.

In figure 9, we show the net mass flows for the thermal transpiration and Poiseuille flows. In panels (a,b), $\mathcal{M}_T$ and $\mathcal{M}_P$ given by (2.17) are shown, respectively, while in panels (c,d), their ratios to the net mass flows for the case of the Boltzmann equation, say $\mathcal{M}_{T,B}$ and $\mathcal{M}_{P,B}$, are shown. The quantity $\mathcal{M}_T$ exhibits the behaviour corresponding to that for the mass flow profile observed in figure 4. Namely, as k becomes smaller, the enhancement of the flow with the increase of $\hat{\sigma}$ compensates for the decrease of the effective gap width, and consequently the values of the net mass flows are close to each other for different $\hat{\sigma}$ values
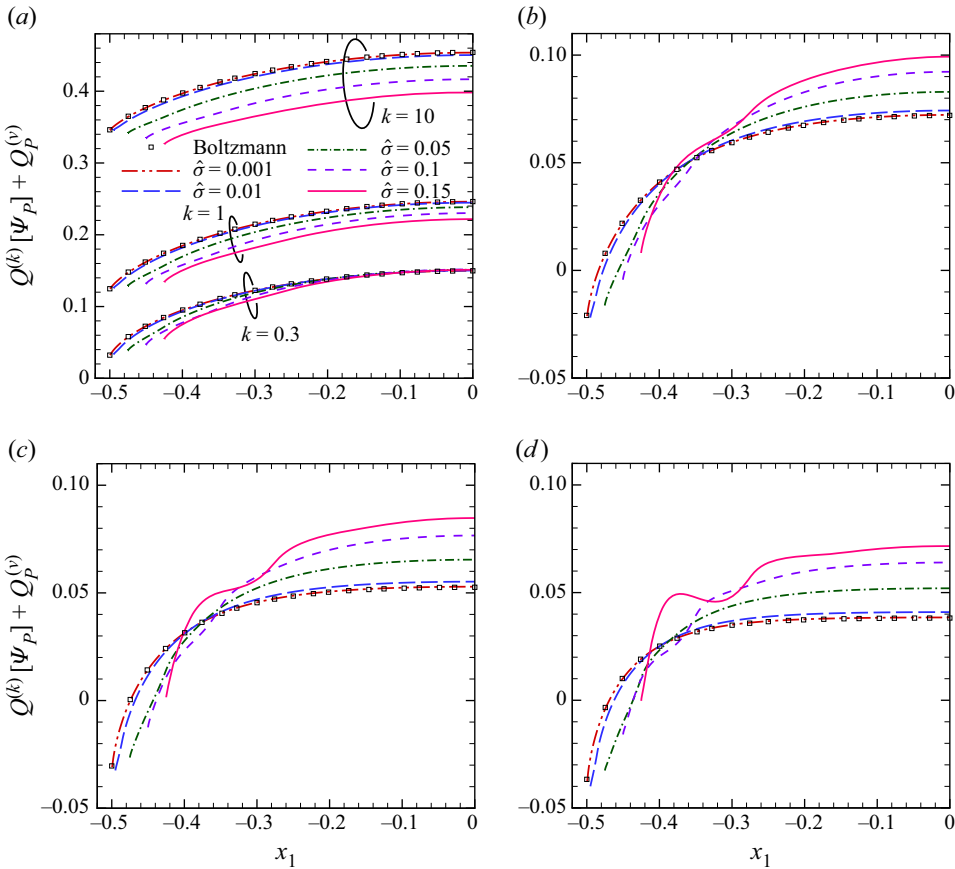
962 A20-18

Figure 7. Profiles of the heat flow of the Poiseuille flow; $Q^{(k)}[\Psi_P] + Q_P^{(v)}$ vs x_1; (*a*) $k = 10$, 1 and 0.3, (*b*) $k = 0.1$, (*c*) $k = 0.07$ and (*d*) $k = 0.05$.

(e.g. for $k = 0.1$ and 0.07). With further decrease of k, the mass flow rate is smaller for larger $\hat{\sigma}$ again because the flow decreases in the central part of the gap. For the Poiseuille flow, when $\hat{\sigma}$ is small, the Knudsen minimum is clearly observed (see panel *b*), which is attributed to the fact that the braking effect due to the plate becomes smaller both as $k \to 0$ and $k \to \infty$ (more thorough explanation is found in the literature). On the other hand, as is also pointed out in Wu *et al.* (2016) and Sheng *et al.* (2020) for the force-driven flows, the plot becomes flatter for larger $\hat{\sigma}$ and the Knudsen minimum becomes more invisible. This is because the flow is not enhanced in the central part of the gap as k becomes smaller; see the plot curves for $\hat{\sigma} = 0.1$ or 0.15 in figure 5(*c*–*e*), which are almost unchanged. In figure 9(*e*,*f*), we show the following quantities:

$$k_* = \frac{k}{1 - \hat{\sigma}}, \quad \mathcal{M}_{\beta,*} = \frac{\mathcal{M}_\beta}{(1 - \hat{\sigma})^2} \quad (\beta = T, P), \quad (4.3)$$

introduced by the conversion which corresponds to the replacement of the reference length D by $D - \sigma$. As k_* becomes larger, the plots for different $\hat{\sigma}$ values exhibit the common trend, which implies that the behaviour of the gas for large Knudsen numbers can be characterized well in terms of the length $D - \sigma$. This is consistent with the explanation of the mass flow for the thermal transpiration flow given in the third paragraph of this section.
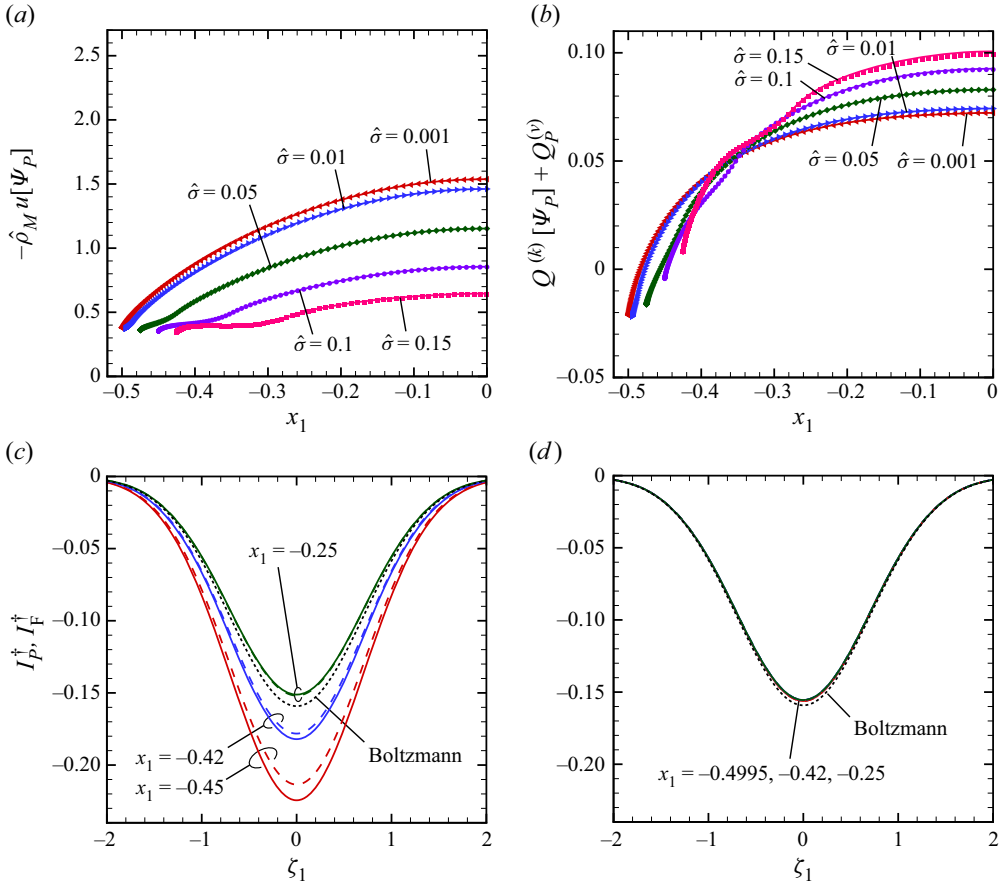
Figure 8. Comparison between the pressure-driven and force-driven Poiseuille flows for the mass flow, heat flow and marginal source term for $k = 0.1$; (a) $\hat{\rho}_M u[\Psi_P]$, (b) $Q^{(k)}[\Psi_P] + Q_P^{(v)}$, (c) $I_P^\dagger$ and $I_F^\dagger$ for $\hat{\sigma} = 0.1$ and (d) $I_P^\dagger$ and $I_F^\dagger$ for $\hat{\sigma} = 0.001$. In (a,b), the symbols indicate the pressure-driven case, while the solid lines the force-driven case. In (c,d), the solid lines indicate the pressure-driven case, while the dashed lines the force-driven case.

Figures 10–12 show the VDF Ψ_T for the degree of gas rarefaction $k = 0.1$, 1 and 10 at three spatial points $x_1 = -(1 - \hat{\sigma})/2$, -0.25 and 0 as functions of the normal velocity component ζ_1 with (ζ_2, ζ_3) being fixed at $(1.106, 0)$. In the figures, the close-ups of the VDFs at the boundary near $\zeta_1 = 0$ are also shown in panel (b) of each figure. First, the following overall behaviour similar to the case of the Boltzmann equation is observed:

(a) There is a jump discontinuity at $\zeta_1 = 0$ on the boundary $x_1 = -(1 - \hat{\sigma})/2$.
(b) When k is small, the discontinuity is small and the VDFs behave moderately in the gas.
(c) When k is large, the VDFs are localized around $\zeta_1 = 0$ including in the gas.

However, for the finite molecular size $\hat{\sigma} \neq 0$, the VDFs deviate considerably from those for the Boltzmann equation for $\zeta_1 < 0$ near the origin on the boundary even when $\hat{\sigma}$ is small (see panel (b) of each figure). As $\hat{\sigma}$ is decreased, while the values of the macroscopic quantities approach those for the Boltzmann equation uniformly in x_1 (see, e.g. figures 4 and 5), the VDFs exhibit non-uniform approach in (x_1, ζ_1). In the following, we consider
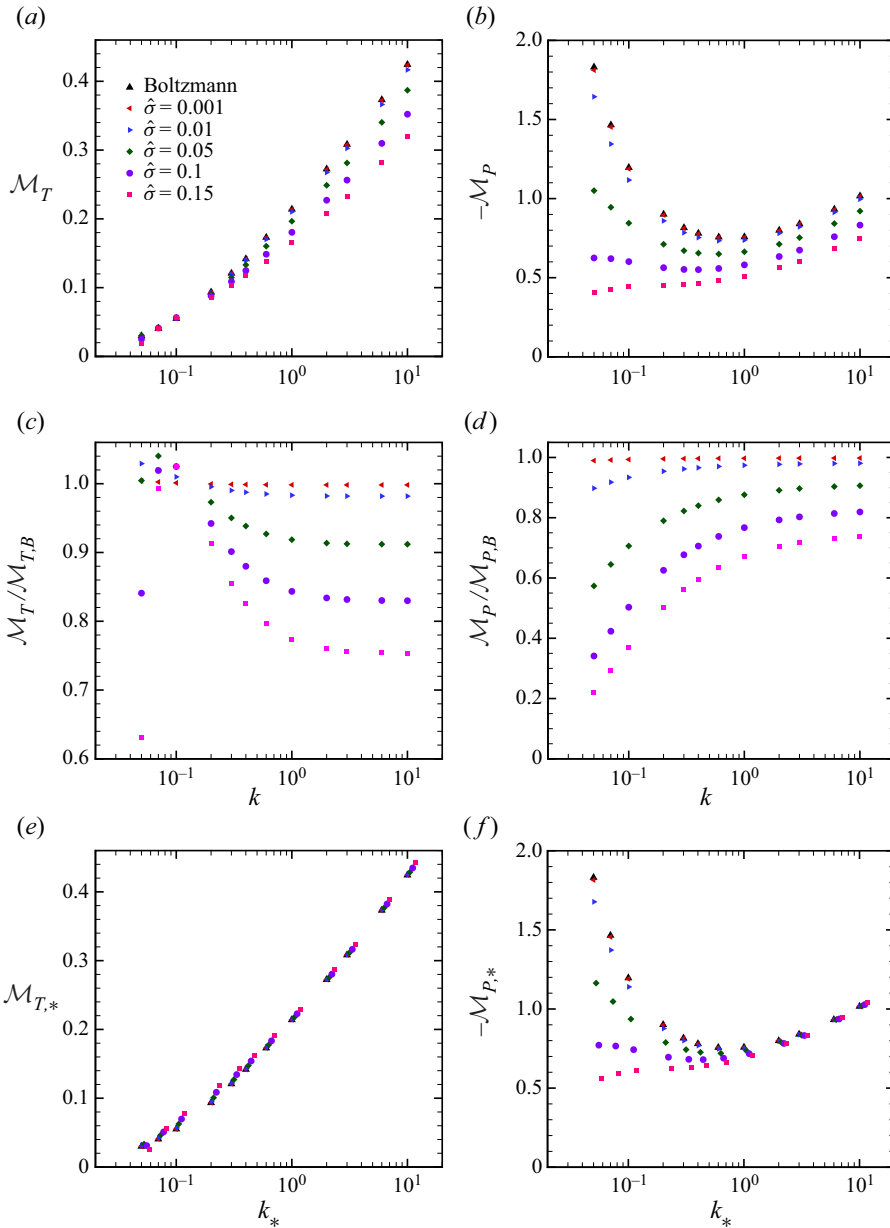
962 A20-20

Figure 9. Quantities related to the net mass flows for the thermal transpiration and Poiseuille flows; (*a*) $\mathcal{M}_T$, (*b*) $\mathcal{M}_P$, (*c*) $\mathcal{M}_T/\mathcal{M}_{T,B}$, (*d*) $\mathcal{M}_P/\mathcal{M}_{P,B}$, (*e*) $\mathcal{M}_{T,*}$ and (*f*) $\mathcal{M}_{P,*}$.

the cause of this behaviour of the VDFs with the aid of the expression (3.1*b*). Since the first term on the right-hand side of (3.1*b*) is exponentially small for $|\zeta_1| \ll 1$, we only have to examine the second term. As in the case of the Boltzmann equation, the integral $C(\Psi_T)$, the collision frequency ν and the source term I_T are smooth in velocity ζ (or ζ_1) also for finite $\hat{\sigma}$, which can be confirmed actually from the numerical results. Thus it is the exponential function that induces the steep variation of Ψ_T in $\zeta_1 < 0$ near the origin. Taking into account the expression of the argument of the exponential function, we see
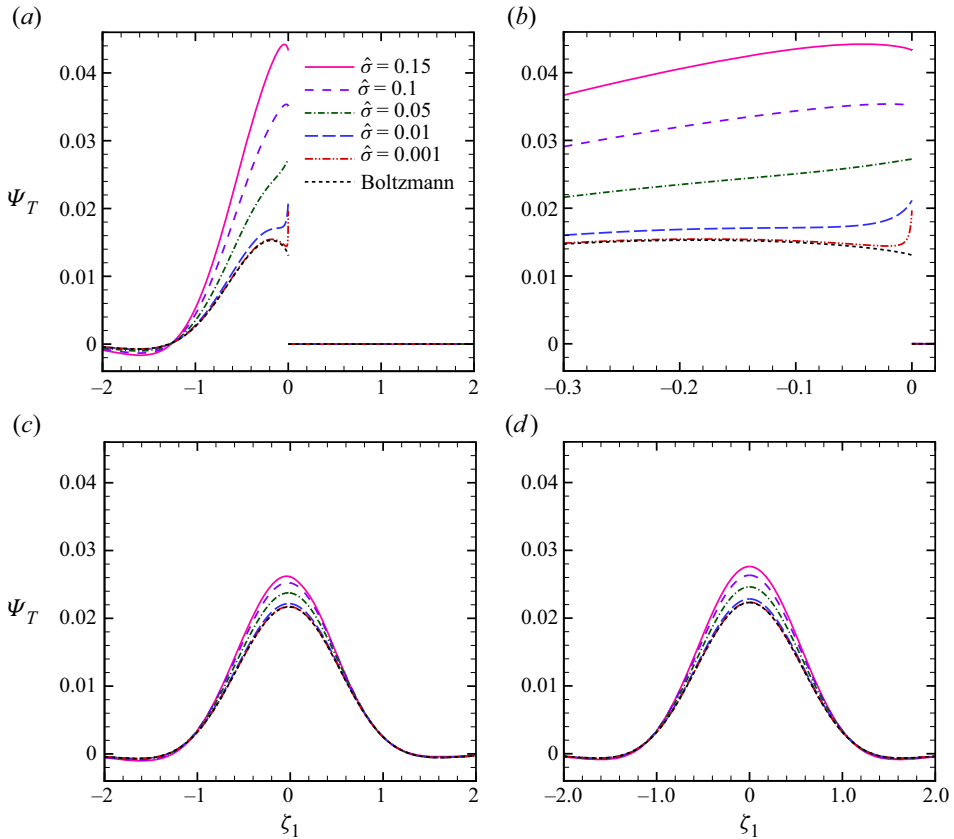
Figure 10. The VDF Ψ_T at $(\zeta_2, \zeta_3) = (1.106, 0)$ for $k = 0.1$; (*a*) $x_1 = -(1 - \hat{\sigma})/2$, (*b*) close-up of (*a*), (*c*) $x_1 = -0.25$ and (*d*) $x_1 = 0$.

that only the integrand in the range $|s + (1 - \hat{\sigma})/2| \lesssim k|\zeta_1|$ actually contributes to the integral with respect to s. In the meantime, $C(\Psi_T)$ and ν vary significantly in x_1 in the region within $O(\hat{\sigma})$ from the boundary, as figure 13 implies. Thus, for $|\zeta_1| \lesssim \hat{\sigma}/k$, Ψ_β is determined from $C(\Psi_\beta)$ and ν substantially affected by the boundary and accordingly its value may deviate largely from that for the case of the Boltzmann equation. To confirm the estimate, we show the deviation of the VDF Ψ_T from that for the case of the Boltzmann equation $\Psi_{T,B}$, say $\Delta\Psi_T = \Psi_T - \Psi_{T,B}$, normalized by its value at $\zeta_1 = -0$ in figure 14. When they are plotted as functions of $k\zeta_1/\hat{\sigma}$, they overlap well with each other for large k and small $\hat{\sigma}$. This supports the above estimate. Note that Ψ_P also has the features described in this paragraph although their figures are omitted.

The comparison of the results shown in this section with other approaches like molecular dynamics (MD) simulation is not carried out here since, unfortunately, it is difficult to find the simulation result of a corresponding system such as molecules under the dense gas condition confined in a channel joined to two reservoirs maintained at different temperature and pressure. However, instead, let us mention some known correspondences between results obtained by the Enskog equation and MD, which support the description of phenomena in dense gases based on the kinetic theory:

(i) It is known that the profile of the reference density obtained from the Enskog equation, $\hat{\rho}_M(x_1)$ in the present paper, agrees well with that obtained by MD simulation (see, e.g. figure 6 in Frezzotti 1997).
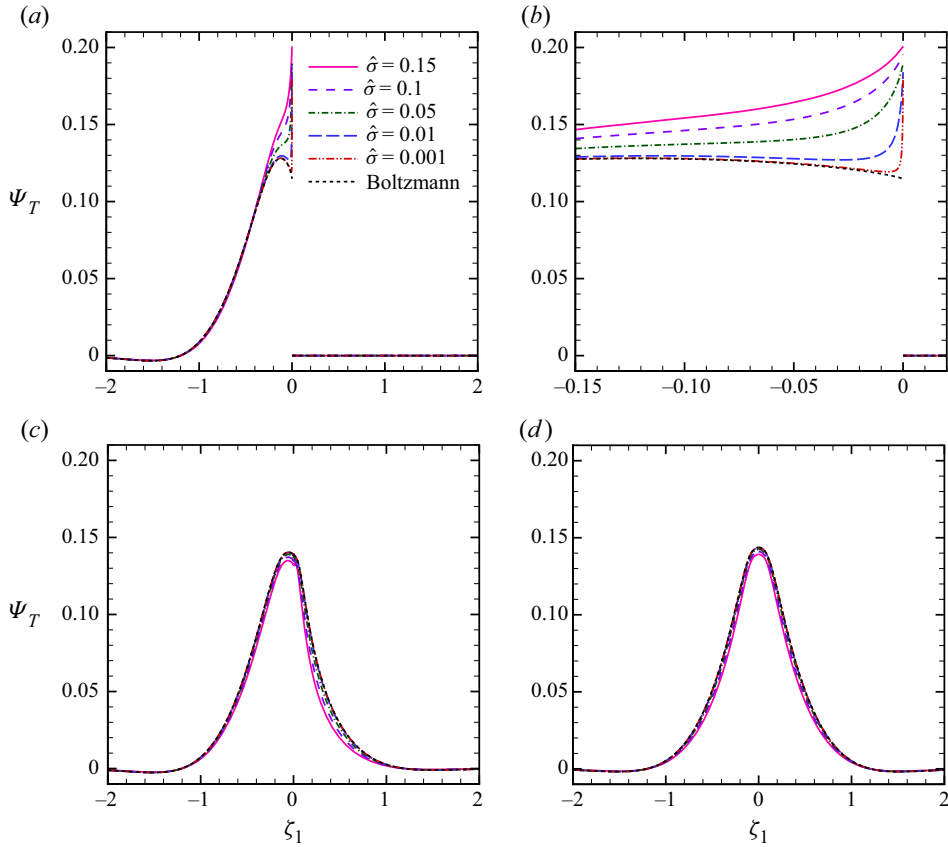
962 A20-22

Figure 11. The VDF Ψ_T at $(\zeta_2, \zeta_3) = (1.106, 0)$ for $k = 1$; (*a*) $x_1 = -(1 - \hat{\sigma})/2$, (*b*) close-up of (*a*), (*c*) $x_1 = -0.25$ and (*d*) $x_1 = 0$.

(ii) For the force-driven flow, it is demonstrated in Sheng *et al.* (2020) that the velocity profile obtained from the Enskog equation agrees well with that obtained by MD simulation (see figures 5 and 6 in the reference).

(iii) As for the thermal response, heat flow as well as the profiles of stress, density and temperature between two parallel plates kept at different constant temperatures obtained from the Enskog equation agree well with those obtained by MD simulation (see Frezzotti 1999).

5. Concluding remarks

We have investigated the thermal transpiration and Poiseuille flows of a dense gas between two parallel plates based on the Enskog equation under the diffuse reflection boundary condition. The problem was linearized around the local equilibrium state that is achieved in the absence of driving sources. Then, the reduced spatially one-dimensional problems were solved numerically by a method based on the integral formulation combined with the fast Fourier spectral method for the computation of the Enskog collision integral. Our findings in the present work are summarized as follows:

(i) In contrast to the case of an ideal gas, the density and the gradients of pressure and normal stress component in the flow direction are not uniform in the direction
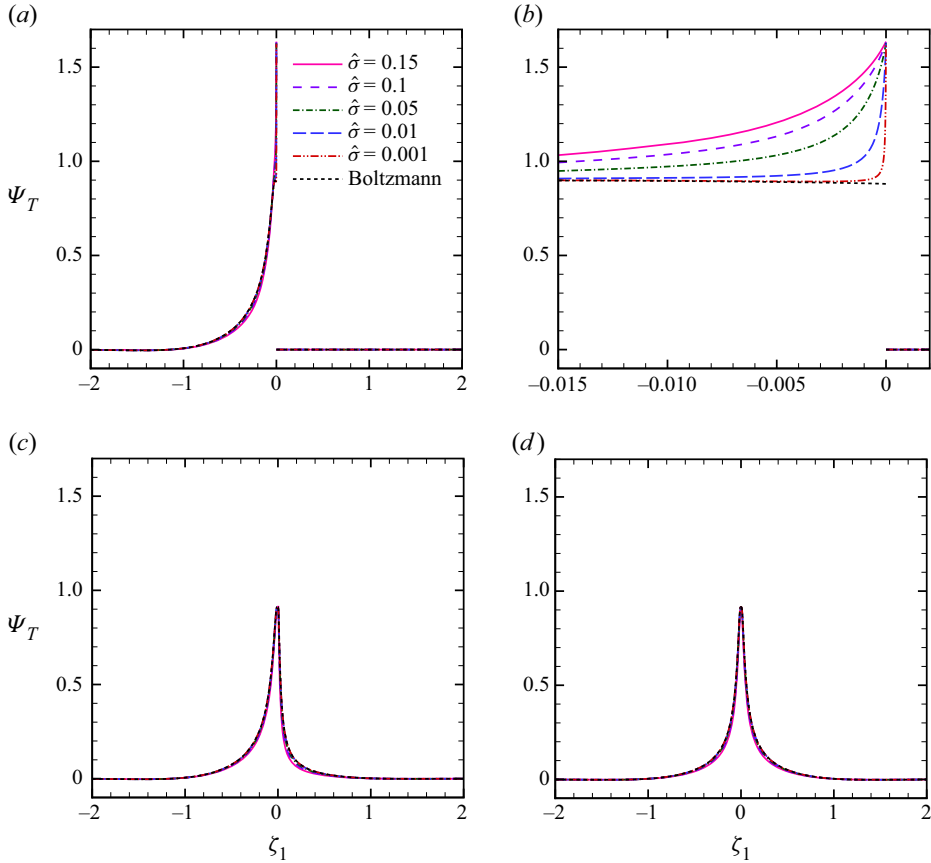
962 A20-23

Figure 12. The VDF Ψ_T at $(\zeta_2, \zeta_3) = (1.106, 0)$ for $k = 10$; (*a*) $x_1 = -(1 - \hat{\sigma})/2$, (*b*) close-up of (*a*), (*c*) $x_1 = -0.25$ and (*d*) $x_1 = 0$.

normal to the plates for a dense gas. The non-uniformity or significant variation has been observed near the boundary within a distance of the order of the molecular diameter for various quantities for a dense gas. The non-uniform normal stress gradient contributes to the acceleration or deceleration of the thermal transpiration flow for small Knudsen numbers.

(ii) The behaviour of mass and heat flows as well as net mass flows has been clarified for various Knudsen numbers and ratios of the molecular diameter to the distance between the plates.

(iii) In the analysis of the Poiseuille flow, most characteristics of the force-driven flow with a small force are recovered. However, for the case of a dense gas, differences between the force-driven and the present pressure-driven flows are observed even within the linearized regime for small force and pressure gradient, especially at the microscopic level.

(iv) The behaviour of VDFs, in particular, the way they approach those for the Boltzmann equation as the molecular diameter becomes smaller, has been clarified.
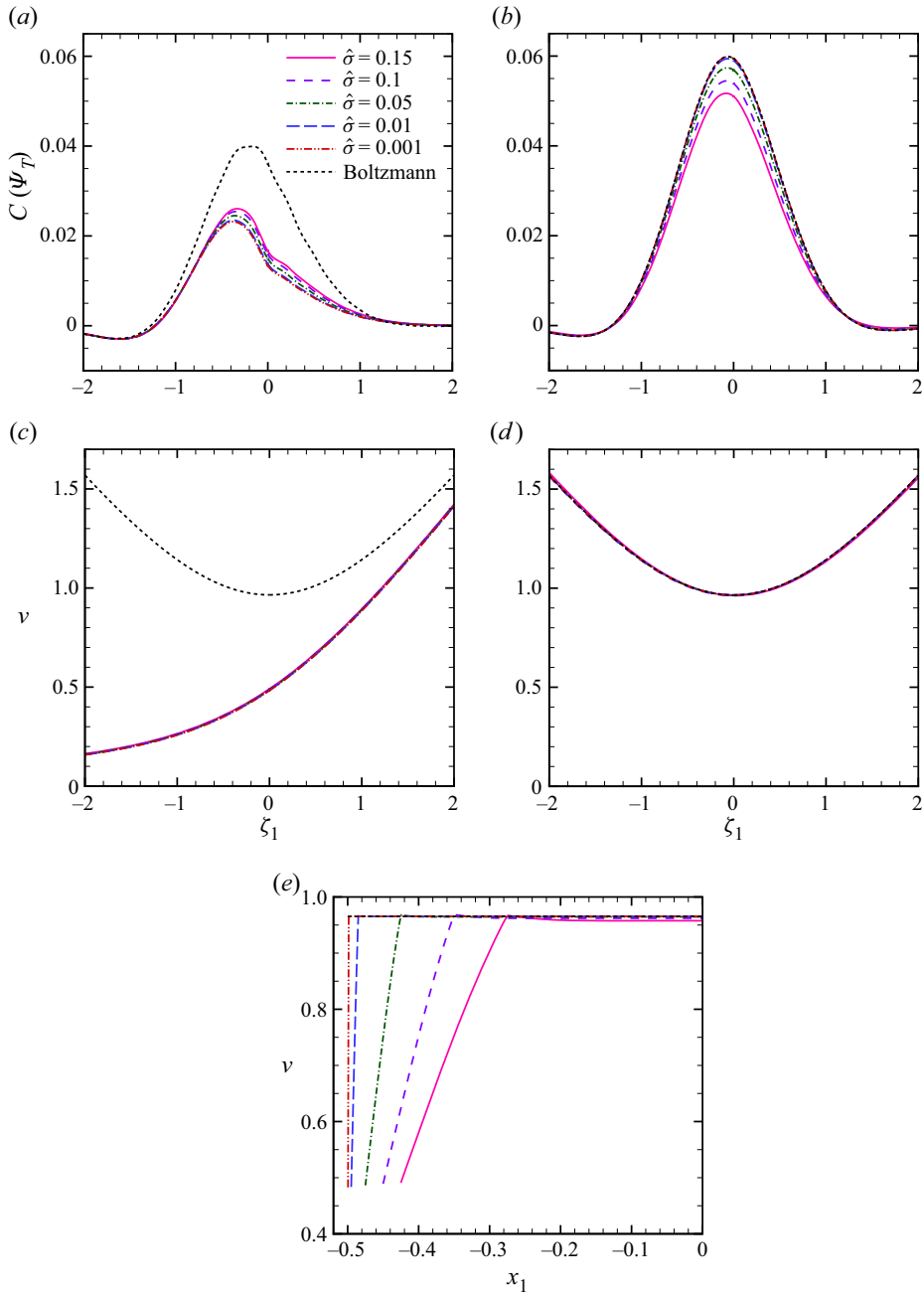
962 A20-24

Figure 13. Plots of the collision integral $C(\Psi_T)$ and the collision frequency ν at $(\zeta_2, \zeta_3) = (1.106, 0)$ for $k = 1$; (a) $C(\Psi_T)$ at $x_1 = -(1 - \hat{\sigma})/2$, (b) $C(\Psi_T)$ at $x_1 = -0.25$, (c) ν at $x_1 = -(1 - \hat{\sigma})/2$, (d) ν at $x_1 = -0.25$ and (e) ν at $\zeta_1 = 0$.
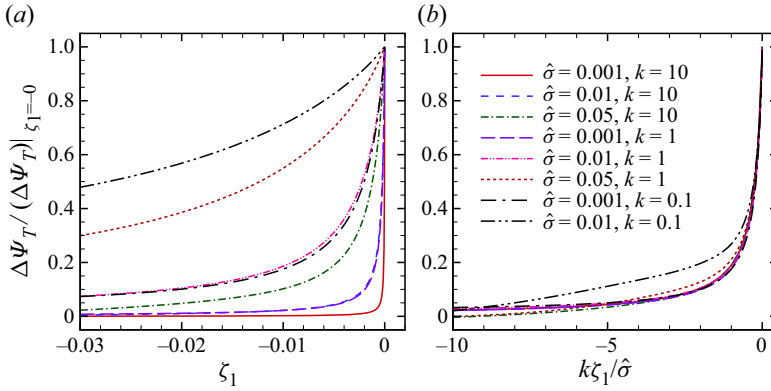
962 A20-25

Figure 14. Plots of the normalized deviation of the VDF for the Enskog equation from that for the Boltzmann equation; $\Delta\Psi_T/(\Delta\Psi_T)|_{\zeta_1=-0}$ at $(\zeta_2, \zeta_3) = (1.106, 0)$; (*a*) vs ζ_1 and (*b*) vs $k\zeta_1/\hat{\sigma}$.

Declaration of interests. The author reports no conflict of interest.

Author ORCIDs.

Masanari Hattori https://orcid.org/0000-0002-5482-0210.

Appendix A. Outline of linearization procedure

In this appendix, we summarize the outline of the linearization procedure for the Enskog equation.

A.1. *Reference equilibrium state*

First, substitute $\hat{f} = \hat{M} = \hat{\rho}_M(x_1)E(\zeta)$ into (2.1*a*). Then, the left-hand side of (2.1*a*) is recast as

$$[\text{Left-hand side of } (2.1a)] = \zeta_1 E(\zeta)\frac{\mathrm{d}\hat{\rho}_M(x_1)}{\mathrm{d}x_1}. \tag{A1}$$

On the other hand, the right-hand side of (2.1*a*) is transformed as

[Right-hand side of (2.1*a*)]

$$= \frac{1}{k2\sqrt{2\pi}} \int \left[\hat{Y}\left(\hat{\rho}_M\left(x_1 + \frac{1}{2}\hat{\sigma}k_1\right); \eta_0 \right) \hat{\rho}_M(x_1 + \hat{\sigma}k_1)E(\zeta_*')\hat{\rho}_M(x_1)E(\zeta') \right.$$

$$\left. - \hat{Y}\left(\hat{\rho}_M\left(x_1 - \frac{1}{2}\hat{\sigma}k_1\right); \eta_0 \right) \hat{\rho}_M(x_1 - \hat{\sigma}k_1)E(\zeta_*)\hat{\rho}_M(x_1)E(\zeta) \right] (\hat{V}\cdot k)H(\hat{V}\cdot k)\,\mathrm{d}k\,\mathrm{d}\zeta_*$$

$$= -\frac{1}{k2\sqrt{2\pi}} \int \hat{Y}\left(\hat{\rho}_M\left(x_1 - \frac{1}{2}\hat{\sigma}k_1\right); \eta_0 \right) \hat{\rho}_M(x_1 - \hat{\sigma}k_1)\hat{\rho}_M(x_1)$$

$$\times (\hat{V}\cdot k)[H(-\hat{V}\cdot k) + H(\hat{V}\cdot k)]E(\zeta_*)E(\zeta)\,\mathrm{d}k\,\mathrm{d}\zeta_*$$

$$= \frac{1}{k2\sqrt{2\pi}} \int \hat{Y}\left(\hat{\rho}_M\left(x_1 - \frac{1}{2}\hat{\sigma}k_1\right); \eta_0 \right) \hat{\rho}_M(x_1 - \hat{\sigma}k_1)\hat{\rho}_M(x_1)$$

$$\times (\zeta_1 k_1 + \zeta_2 k_2 + \zeta_3 k_3)E(\zeta)\,\mathrm{d}k$$

962 A20-26

$$= \frac{2\pi}{k2\sqrt{2\pi}} \hat{\rho}_M(x_1) \zeta_1 E(\zeta) \int_{-1}^{1} \hat{Y}\left(\hat{\rho}_M\left(x_1 - \frac{1}{2}\hat{\sigma}z\right); \eta_0\right) \hat{\rho}_M(x_1 - \hat{\sigma}z)z\, \mathrm{d}z$$

$$= \zeta_1 E(\zeta) J_1[\hat{\rho}_M](x_1), \tag{A2}$$

where J_1 is given in Appendix B. Note that (a) at the second equality, $E(\zeta_*')E(\zeta') = E(\zeta_*)E(\zeta)$ is used and change of a variable $\boldsymbol{k} \to -\boldsymbol{k}$ is applied for the first term in the integrand; (b) at the third equality, $H(-\hat{\boldsymbol{V}} \cdot \boldsymbol{k}) + H(\hat{\boldsymbol{V}} \cdot \boldsymbol{k}) = 1$ is used and the integration over $\boldsymbol{\zeta}_*$ is carried out; (c) at the fourth equality, with the x_1 direction as the polar direction, the integration with respect to the azimuthal angle of $\boldsymbol{k}$ is carried out (then the contribution from the parts multiplied by $\zeta_2 k_2$ and $\zeta_3 k_3$ vanish) and that with respect to the polar angle of $\boldsymbol{k}$ is expressed as the integral with respect to the variable z.

Equating (A1) and (A2), we have the equation (2.5a) for the density $\hat{\rho}_M(x_1)$. Since $\hat{M}$ is a Maxwellian, it satisfies the diffuse reflection boundary condition (2.1g) with the plate temperature $\hat{T}_w(x_2)$ being replaced by the reference temperature 1. Substituting $\hat{f} = \hat{M} = \hat{\rho}_M(x_1)E(\zeta)$ into the condition (2.1j) for average density, immediately we have (2.5b). When the density $\hat{\rho}_M(x_1)$ satisfies (2.5), the local equilibrium state $\hat{M} = \hat{\rho}_M(x_1)E(\zeta)$ satisfies the Enskog equation (2.1a) in the domain $-(1 - \hat{\sigma})/2 < x_1 < (1 - \hat{\sigma})/2$.

A.2. *Perturbation*

Now, let us introduce the perturbation, Φ, and express $\hat{f}$ as $\hat{f} = \hat{M} + \Phi$. Then, subtracting Enskog equation (2.1a) for $\hat{f} = M$ from that for $\hat{f} = \hat{M} + \Phi$, we have

$$\zeta_1 \frac{\partial \Phi}{\partial x_1} + \zeta_2 \frac{\partial \Phi}{\partial x_2} = \frac{1}{k}[\hat{Q}(\hat{M} + \Phi) - \hat{Q}(\hat{M})] = \frac{1}{k}L(\Phi) + O(\Phi^2), \tag{A3}$$

where L is the collision operator linearized around the reference local equilibrium state $\hat{M}(x_1, \boldsymbol{\zeta})$. The expression (2.8) of L is obtained in a straightforward way by using the transformation $\hat{Y}(\hat{\rho})\hat{f}\hat{f} = [\hat{Y}(\hat{\rho}_M) + \langle\Phi\rangle\hat{Y}_1(\hat{\rho}_M) + O(\Phi^2)](\hat{M} + \Phi)(\hat{M} + \Phi) = \hat{Y}(\hat{\rho}_M)\hat{M}\hat{M} + \{\hat{Y}(\hat{\rho}_M)(\hat{M}\Phi + \Phi\hat{M}) + \langle\Phi\rangle\hat{Y}_1(\hat{\rho}_M)\hat{M}\hat{M}\} + O(\Phi^2)$ (see also (2.10)).

Subtracting the boundary condition (2.1g) or the condition (2.1j) for average density for $\hat{f} = M$ from those for $\hat{f} = \hat{M} + \Phi$, respectively, we have

$$\text{b.c.} \quad \Phi = \left[\check{\rho}_w + \hat{\rho}_M\left(\mp\frac{1-\hat{\sigma}}{2}\right)\left(\zeta^2 - \frac{3}{2}\right)c_T x_2\right]E(\zeta) + O(c_T\Phi, \Phi^2),$$

$$\left(\zeta_1 \gtrless 0, \ x_1 = \mp\frac{1-\hat{\sigma}}{2}\right), \tag{A4a}$$

$$\check{\rho}_w = -\frac{1}{2}c_T x_2 \hat{\rho}_M\left(\mp\frac{1-\hat{\sigma}}{2}\right) \mp 2\sqrt{\pi}\int_{\zeta_1 \lessgtr 0}\zeta_1 \Phi\, \mathrm{d}\boldsymbol{\zeta}, \tag{A4b}$$

$$\text{with} \quad \left(\int_{-(1-\hat{\sigma})/2}^{(1-\hat{\sigma})/2}\int \Phi\, \mathrm{d}\boldsymbol{\zeta}\, \mathrm{d}x_1\right)\Bigg|_{x_2=0} = 0. \tag{A4c}$$

Derivation of (A4) is straightforward and parallel to the case of the Boltzmann equation.

A.3. *Form of perturbation*

We need to find the appropriate form of the perturbation Φ such that Φ represents the gradients of temperature and pressure (or stress) and satisfies its equation (A3) and conditions (A4) within the linearized regime.

For the Boltzmann equation, it is known that such a solution Φ can be sought in the form

$$\Phi = c_T \left[x_2 E(\zeta) \left(-1 + \left(\zeta^2 - \frac{3}{2} \right) \right) + \bar{\Psi}_T(x_1, \zeta) \right] + \bar{c}_P \left[x_2 E(\zeta) + \bar{\Psi}_P(x_1, \zeta) \right], \quad \text{(A5)}$$

where $\bar{c}_P$ is a small constant and $\bar{\Psi}_T$ and $\bar{\Psi}_P$ are odd in ζ_2. The bar is attached to discriminate the quantities from those for the Enskog equation. Calculating the temperature $\hat{T}$ and the stress $\hat{p}_{22}$ with $\hat{f} = \hat{M} + \Phi$ for the Boltzmann equation, we have $\hat{T} = 1 + c_T x_2$ and $\hat{p}_{22} = 1 + \bar{c}_P x_2 (= \hat{p})$ within the linearized regime (the negligible $O(\bar{c}_P^2, c_T^2)$ error terms are dropped in these expressions). We see that $\bar{c}_P$ corresponds to the gradient of stress (or pressure) in the x_2 direction. The problem for Φ is rewritten to those for $\bar{\Psi}_T$ and $\bar{\Psi}_P$.

Unfortunately, for the case of Enskog equation, the form (A5) cannot satisfy the equation (A3) and a modification is required. A clue for an appropriate modification is that the reference state $\hat{M}$ is a Maxwellian with uniform temperature but variable density profile in the x_1 direction for the case of Enskog equation. We attempt to make the perturbation have the corresponding properties too. Accordingly, we introduce perturbed density profile, say $\hat{\omega}_T(x_1)$ and $\hat{\omega}_P(x_1)$, as well while keeping the temperature is constant in x_1. This leads to the introduction of the form (2.4c) of Φ, i.e. $\Phi = c_T \left\{ x_2 E(\zeta) \left[\hat{\omega}_T(x_1) + (\zeta^2 - \frac{3}{2}) \hat{\rho}_M(x_1) \right] + \Psi_T(x_1, \zeta) \right\} + c_P \left[x_2 E(\zeta) \hat{\omega}_P(x_1) + \Psi_P(x_1, \zeta) \right]$. Note that the case of Boltzmann equation corresponds to the case $\hat{\rho}_M(x_1) \equiv 1$, $\hat{\omega}_T(x_1) \equiv -1$ and $\hat{\omega}_P(x_1) \equiv 1$.

Calculating the temperature $\hat{T}$ and the stress $\hat{p}_{22}$ with $\hat{f} = \hat{M} + \Phi$ for the Enskog equation, we have $\hat{T} = 1 + c_T x_2$ and

$$\begin{aligned}
\hat{p}_{22} &= \hat{p}_{22}^{(k)} + \hat{p}_{22}^{(v)} (\neq \hat{p}) \\
&= [\hat{\rho}_M(x_1) + P_{22,M}^{(v)}(x_1)] + c_T x_2 [G_{22,T}^{(k)}(x_1) \\
&\quad + G_{22,T}^{(v)}(x_1)] + c_P x_2 [G_{22,P}^{(k)}(x_1) + G_{22,P}^{(v)}(x_1)], \quad \text{(A6)}
\end{aligned}$$

within the linearized regime (the negligible $O(c_P^2, c_T^2)$ error terms are dropped in these expressions), where $G_{22,T}^{(k)} = \hat{\rho}_M(x_1) + \hat{\omega}_T(x_1)$ and $G_{22,P}^{(k)} = \hat{\omega}_P(x_1)$, and the expressions of the stress contribution $P_{22,M}^{(v)}$ and the gradients $G_{22,T}^{(v)}$ and $G_{22,P}^{(v)}$ are given in Appendix C. The calculation of $\hat{p}_{22}^{(k)}$ is parallel to the case of Boltzmann equation. As for that of $\hat{p}_{22}^{(v)}$ (2.3f), thanks to the explicit functional form of Φ in ζ except the parts of $\Psi_{T,P}$, the integration with respect to ζ and ζ_* can be carried out firstly with k and $\hat{\alpha}$ being fixed and that with respect to the azimuthal angle of k can also be carried out subsequently. The contribution from $\Psi_{T,P}$ vanishes due to their oddness in ζ_2. Now, in accordance with the nature of the Poiseuille and thermal transpiration flows, we require that

$$\frac{1}{1 - \hat{\sigma}} \int_{-(1-\hat{\sigma})/2}^{(1-\hat{\sigma})/2} [G_{22,P}^{(k)}(x_1) + G_{22,P}^{(v)}(x_1)] \, dx_1 = 1, \quad \text{(A7a)}$$

$$\frac{1}{1-\hat{\sigma}} \int_{-(1-\hat{\sigma})/2}^{(1-\hat{\sigma})/2} [G_{22,T}^{(k)}(x_1) + G_{22,T}^{(v)}(x_1)] \, dx_1 = 0. \tag{A7b}$$

See also the item (ii) in § 2.4. Under (A7), c_P corresponds to the gradient of stress in the x_2 direction averaged in the x_1 direction (see (A6)). Substituting the expressions of $G_{22,P}^{(k,v)}$ and $G_{22,T}^{(k,v)}$ into (A7a) and (A7b), they reduce to the subsidiary conditions (2.6c) and (2.6b) for $\hat{\omega}_P$ and $\hat{\omega}_T$. Their derivations are straightforward.

A.4. *Compatibility of perturbation*

Finally, we have to check if the solution Φ of the equation (A3) under the conditions (A4) can be sought without any inconsistency in the form (2.4c) within negligible error in the linearized regime.

Since $\Phi|_{x_2=0} = c_T \Psi_T + c_P \Psi_P$ and $\Psi_{T,P}$ is considered to be odd in ζ_2, the condition (A4c) for average density is satisfied automatically. Substituting (2.4c) into the boundary condition (A4a) and (A4b) leads to the homogeneous boundary condition (2.7b) for $\Psi_{T,P}$, whose derivation is parallel to the case of Boltzmann equation. It remains to check the compatibility with the equation (A3).

Substituting (2.4c) into the equation (A3) for Φ, its left-hand side is recast as

$$
\begin{aligned}
\zeta_1 \frac{\partial \Phi}{\partial x_1} + \zeta_2 \frac{\partial \Phi}{\partial x_2} = c_T &\left\{ x_2 \zeta_1 E(\zeta) \left[\frac{d\hat{\omega}_T(x_1)}{dx_1} + \left(\zeta^2 - \frac{3}{2} \right) \frac{d\hat{\rho}_M(x_1)}{dx_1} \right] \right. \\
&\left. + \zeta_1 \frac{\partial \Psi_T}{\partial x_1}(x_1, \zeta) + \zeta_2 E(\zeta) \left[\hat{\omega}_T(x_1) + \left(\zeta^2 - \frac{3}{2} \right) \hat{\rho}_M(x_1) \right] \right\} \\
&+ c_P \left\{ x_2 \zeta_1 E(\zeta) \frac{d\hat{\omega}_P(x_1)}{dx_1} + \zeta_1 \frac{\partial \Psi_P}{\partial x_1}(x_1, \zeta) + \zeta_2 E(\zeta) \hat{\omega}_P(x_1) \right\}. \quad (A8)
\end{aligned}
$$

We see that the terms in (A8) can be classified into three different kinds of terms according to their functional form with respect to x_2 and ζ: (I) $c_T x_2 \zeta_1 E(\zeta)(\zeta^2 - 3/2) \, d\hat{\rho}_M(x_1)/dx_1$, (II) $c_{T,P} x_2 \zeta_1 E(\zeta) \, d\hat{\omega}_{T,P}(x_1)/dx_1$, (III) $c_T \left\{ \zeta_1 \partial \Psi_T(x_1, \zeta)/\partial x_1 + \zeta_2 E(\zeta) \left[\hat{\omega}_T(x_1) + (\zeta^2 - \frac{3}{2}) \hat{\rho}_M(x_1) \right] \right\}$ and $c_P \{ \zeta_1 \partial \Psi_P(x_1, \zeta)/\partial x_1 + \zeta_2 E(\zeta) \hat{\omega}_P(x_1) \}$. The terms of third kind are odd in ζ_2 and do not depend on x_2.

For the right-hand side of (A3), first let us rewrite the form (2.4c) as $\Phi = (c_T \Psi_T + c_P \Psi_P) + c_T x_2 E(\zeta^2 - \frac{3}{2})\hat{\rho}_M + x_2 E(c_T \hat{\omega}_T + c_P \hat{\omega}_P)$. Then substituting it into the right-hand side of (A3) and making use of the linearity of the collision operator L, we have

$$
\begin{aligned}
\frac{1}{k} L(\Phi) = \frac{1}{k} L(c_T \Psi_T + c_P \Psi_P) + \frac{1}{k} L \left(c_T x_2 E \left(\zeta^2 - \frac{3}{2} \right) \hat{\rho}_M \right) \\
+ \frac{1}{k} L(x_2 E(c_T \hat{\omega}_T + c_P \hat{\omega}_P)), \quad (A9a)
\end{aligned}
$$

where

$$\frac{1}{k} L(c_T \Psi_T + c_P \Psi_P) = c_T \frac{1}{k} L(\Psi_T) + c_P \frac{1}{k} L(\Psi_P), \tag{A9b}$$

962 A20-29

$$\frac{1}{k}L\left(c_T x_2 E\left(\zeta^2 - \frac{3}{2}\right)\hat{\rho}_M\right)$$

$$= c_T x_2 \zeta_1 E(\zeta)\left(\zeta^2 - \frac{3}{2}\right)J_1[\hat{\rho}_M](x_1) - c_T \frac{\hat{\sigma}E(\zeta)}{k2\sqrt{2\pi}}J_3[\hat{\rho}_M](x_1, \boldsymbol{\zeta}), \tag{A9c}$$

$$\frac{1}{k}L(x_2 E(c_T \hat{\omega}_T + c_P \hat{\omega}_P))$$

$$= c_T x_2 \zeta_1 E(\zeta)K_1[\hat{\omega}_T, \hat{\rho}_M](x_1) - c_T \frac{\hat{\sigma}E(\zeta)}{k2\sqrt{2\pi}}\zeta_2 K_3[\hat{\omega}_T, \hat{\rho}_M](x_1)$$

$$+ c_P x_2 \zeta_1 E(\zeta)K_1[\hat{\omega}_P, \hat{\rho}_M](x_1) - c_P \frac{\hat{\sigma}E(\zeta)}{k2\sqrt{2\pi}}\zeta_2 K_3[\hat{\omega}_P, \hat{\rho}_M](x_1), \tag{A9d}$$

and the integrals J_1, J_3, K_1 and K_3 are given in Appendix B. Derivation of (A9c) and (A9d) can be done straightforwardly in the similar way as (A2), where the same kind of operations (see the items (a)–(c) after (A2)) can be used again. When the arguments proportional to x_2 are substituted into the collision operator $L(\psi)$ ((A9c) and (A9d)), due to the position displacements $\boldsymbol{x} \pm \hat{\sigma}\boldsymbol{k}$ for ψ and $\boldsymbol{x} \pm (\hat{\sigma}/2)\boldsymbol{k}$ for $\langle\psi\rangle$ (see also (2.8)), factors with $x_2 \pm \hat{\sigma}k_2$ and $x_2 \pm (\hat{\sigma}/2)k_2$ occur in the integrand of $L(\psi)$. Then, the contribution from parts proportional to x_2 gives the first term of the right-hand side of (A9c) and the first and third terms of the right-hand side of (A9d), and that from parts proportional to $\pm\hat{\sigma}k_2$ and $\pm(\hat{\sigma}/2)k_2$ gives the second term of the right-hand side of (A9c) and the second and fourth terms of the right-hand side of (A9d), respectively.

Corresponding to the classification after (A8), the terms on the right-hand side of (A3), $\frac{1}{k}L(\Phi)$ given in (A9), can also be classified into: (I) $c_T x_2 \zeta_1 E(\zeta)(\zeta^2 - \frac{3}{2})J_1[\hat{\rho}_M](x_1)$, (II) $c_{T,P}x_2\zeta_1 E(\zeta)K_1[\hat{\omega}_{T,P}, \hat{\rho}_M](x_1)$ and (III) $c_{T,P}(1/k)L(\Psi_{T,P})$, $-c_T(\hat{\sigma}E(\zeta)/k2\sqrt{2\pi})J_3[\hat{\rho}_M](x_1, \boldsymbol{\zeta})$ and $-c_{T,P}(\hat{\sigma}E(\zeta)/k2\sqrt{2\pi})\zeta_2 K_3[\hat{\omega}_{T,P}, \hat{\rho}_M](x_1)$. The terms of the third kind can be confirmed to be actually odd in ζ_2.

Finally, we equate (A8) and (A9a) by taking into account the classification (I)–(III) of the terms. For the first kind of terms, because the equation for $\hat{\rho}_M$, $\mathrm{d}\hat{\rho}_M(x_1)/\mathrm{d}x_1 = J_1[\hat{\rho}_M](x_1)$, holds, we find that they nicely cancel out. Equating the second kind of terms, we obtain the equation (2.6) for $\hat{\omega}_{T,P}$. Equating the third kind of terms, the equation (2.7) for $\Psi_{T,P}$ with the source term (2.11) is obtained.

Appendix B. Definitions of J_i and K_i

The integrals J_1, J_2 and J_3 in (2.5a), (2.6b) and (2.11a) are given by

$$J_1[\hat{\rho}_M](x_1) = \frac{1}{k}\sqrt{\frac{\pi}{2}}\hat{\rho}_M(x_1)\int_{-1}^{1}\hat{Y}\left(\hat{\rho}_M(r_m); \eta_0\right)\hat{\rho}_M(r_o)z\,\mathrm{d}z, \tag{B1a}$$

$$J_2[\hat{\rho}_M] = -\frac{\sqrt{\pi}}{4\sqrt{2}k(1-\hat{\sigma})}\int_{-(1-\hat{\sigma})/2}^{(1-\hat{\sigma})/2}\int_{0}^{\hat{\sigma}}\int_{-1}^{1}(1-z^2)\hat{Y}\left(\hat{\rho}_M(r_c); \eta_0\right)$$
$$\times \hat{\rho}_M(r_a)\hat{\rho}_M(r_b)\,\mathrm{d}z\,\mathrm{d}\hat{\alpha}\,\mathrm{d}s, \tag{B1b}$$

$$J_3[\hat{\rho}_M](x_1, \boldsymbol{\zeta}) = \frac{1}{\sqrt{\pi}}\int k_2 \hat{Y}\left(\hat{\rho}_M\left(x_1 + \frac{1}{2}\hat{\sigma}k_1\right); \eta_0\right)$$
$$\times \hat{\rho}_M(x_1 + \hat{\sigma}k_1)\hat{\rho}_M(x_1)Z(\boldsymbol{\zeta}\cdot\boldsymbol{k})\,\mathrm{d}\boldsymbol{k}, \tag{B1c}$$

where

$$r_o = x_1 - \hat{\sigma}z, \quad r_m = x_1 - \frac{1}{2}\hat{\sigma}z, \tag{B2a}$$

$$r_a = s - \hat{\alpha}z, \quad r_b = s + (\hat{\sigma} - \hat{\alpha})z, \quad r_c = s + \left(\frac{1}{2}\hat{\sigma} - \hat{\alpha}\right)z, \tag{B2b}$$

$$Z(t) = \frac{1}{2}(1 - t^2)e^{-t^2} + \frac{\sqrt{\pi}}{2}\left(t^3 - \frac{1}{2}t\right)(1 - \mathrm{erf}(t)), \quad \mathrm{erf}(t) = \frac{2}{\sqrt{\pi}}\int_0^t e^{-\tau^2}\,\mathrm{d}\tau. \tag{B2c}$$

The integrals K_1, K_2 and K_3 in (2.6) and (2.11) are given as follows:

$$K_1[\hat{\omega}_\beta, \hat{\rho}_M](x_1) = \frac{1}{k}\sqrt{\frac{\pi}{2}}\left[\int_{-1}^1 \hat{Y}\left(\hat{\rho}_M(r_m); \eta_0\right)[\hat{\rho}_M(r_o)\hat{\omega}_\beta(x_1) + \hat{\omega}_\beta(r_o)\hat{\rho}_M(x_1)]z\,\mathrm{d}z \right.$$
$$\left. + \int_{-1}^1 \hat{Y}_1\left(\hat{\rho}_M(r_m); \eta_0\right)\hat{\omega}_\beta(r_m)\hat{\rho}_M(r_o)\hat{\rho}_M(x_1)z\,\mathrm{d}z\right], \tag{B3a}$$

$$K_2[\hat{\omega}_\beta, \hat{\rho}_M] = \frac{\sqrt{\pi}}{4\sqrt{2}k(1-\hat{\sigma})}\int_{-(1-\hat{\sigma})/2}^{(1-\hat{\sigma})/2}\int_0^{\hat{\sigma}}\int_{-1}^1 (1-z^2)$$
$$\times \left\{\hat{Y}\left(\hat{\rho}_M(r_c); \eta_0\right)\left[\hat{\rho}_M(r_a)\hat{\omega}_\beta(r_b) + \hat{\omega}_\beta(r_a)\hat{\rho}_M(r_b)\right]\right.$$
$$\left. + \hat{Y}_1\left(\hat{\rho}_M(r_c); \eta_0\right)\hat{\omega}_\beta(r_c)\hat{\rho}_M(r_a)\hat{\rho}_M(r_b)\right\}\mathrm{d}z\,\mathrm{d}\hat{\alpha}\,\mathrm{d}s$$
$$+ \frac{1}{1-\hat{\sigma}}\int_{-(1-\hat{\sigma})/2}^{(1-\hat{\sigma})/2}\hat{\omega}_\beta(s)\,\mathrm{d}s, \tag{B3b}$$

$$K_3[\hat{\omega}_\beta, \hat{\rho}_M](x_1) = \pi\int_{-1}^1 (1-z^2)\left[\hat{Y}\left(\hat{\rho}_M(r_m); \eta_0\right)\hat{\omega}_\beta(r_o)\hat{\rho}_M(x_1)\right.$$
$$\left. + \frac{1}{2}\hat{Y}_1\left(\hat{\rho}_M(r_m); \eta_0\right)\hat{\omega}_\beta(r_m)\hat{\rho}_M(r_o)\hat{\rho}_M(x_1)\right]\mathrm{d}z. \tag{B3c}$$

Appendix C. Definitions of several moments

The functions $P_{11,M}^{(v)}$, $P_{22,M}^{(v)}$, $G_{11,T}^{(v)}$, $G_{22,T}^{(v)}$, $P_{12,\omega_T}^{(v)}$, $P_{12}^{(v)}[\Psi_\beta]$ and $Q^{(v)}[\Psi_\beta]$ in (2.14) and (2.15) are given by

$$\begin{bmatrix} P_{11,M}^{(v)} \\ P_{22,M}^{(v)} \end{bmatrix} = \frac{\sqrt{\pi}}{4\sqrt{2}k}\int_{-1}^1\int_0^{\hat{\sigma}}\begin{bmatrix} 2z^2 \\ 1-z^2 \end{bmatrix}\hat{Y}\left(\hat{\rho}_M(r_C); \eta_0\right)\hat{\rho}_M(r_A)\hat{\rho}_M(r_B)\,\mathrm{d}\hat{\alpha}\,\mathrm{d}z, \tag{C1a}$$

$$\begin{bmatrix} G_{11,T}^{(v)} \\ G_{22,T}^{(v)} \end{bmatrix} = \frac{\sqrt{\pi}}{4\sqrt{2}k}\int_{-1}^1\int_0^{\hat{\sigma}}\begin{bmatrix} 2z^2 \\ 1-z^2 \end{bmatrix}$$
$$\times \left\{\hat{Y}\left(\hat{\rho}_M(r_C); \eta_0\right)\left[\hat{\rho}_M(r_A)\hat{\omega}_T(r_B) + \hat{\omega}_T(r_A)\hat{\rho}_M(r_B)\right]\right.$$
$$+ \hat{Y}_1\left(\hat{\rho}_M(r_C); \eta_0\right)\hat{\omega}_T(r_C)\hat{\rho}_M(r_A)\hat{\rho}_M(r_B)$$
$$\left. + \hat{Y}\left(\hat{\rho}_M(r_C); \eta_0\right)\hat{\rho}_M(r_A)\hat{\rho}_M(r_B)\right\}\mathrm{d}\hat{\alpha}\,\mathrm{d}z, \tag{C1b}$$

962 A20-31

$$P_{12,\omega_T}^{(v)} = \frac{\sqrt{\pi}}{4\sqrt{2}k} \int_{-1}^{1} \int_{0}^{\hat{\sigma}} z(1 - z^2)$$

$$\times \left\{ \hat{Y}\left(\hat{\rho}_M\left(r_C\right); \eta_0\right) \left[(\hat{\sigma} - \hat{\alpha})\hat{\rho}_M(r_A)\hat{\omega}_T(r_B) - \hat{\alpha}\hat{\omega}_T(r_A)\hat{\rho}_M(r_B)\right]\right.$$

$$\left. + \left(\frac{1}{2}\hat{\sigma} - \hat{\alpha}\right)\hat{Y}_1\left(\hat{\rho}_M\left(r_C\right); \eta_0\right)\hat{\omega}_T\left(r_C\right)\hat{\rho}_M(r_A)\hat{\rho}_M(r_B)\right.$$

$$\left. + \left(\frac{1}{2}\hat{\sigma} - \hat{\alpha}\right)\hat{Y}\left(\hat{\rho}_M\left(r_C\right); \eta_0\right)\hat{\rho}_M(r_A)\hat{\rho}_M(r_B)\right\} \, d\hat{\alpha} \, dz, \tag{C1c}$$

$$P_{12}^{(v)}[\Psi_\beta] = \frac{1}{2\sqrt{2\pi}k} \int_0^{\hat{\sigma}} \iint k_1 k_2 \hat{Y}\left(\hat{\rho}_M\left(x_1 + \left(\frac{1}{2}\hat{\sigma} - \hat{\alpha}\right)k_1\right); \eta_0\right)$$

$$\times \left[I_P^{(+)}(\boldsymbol{\zeta} \cdot \boldsymbol{k})\hat{\rho}_M(x_1 - \hat{\alpha}k_1)\Psi_\beta(x_1 + (\hat{\sigma} - \hat{\alpha})k_1, \boldsymbol{\zeta})\right.$$

$$\left. + I_P^{(-)}(\boldsymbol{\zeta} \cdot \boldsymbol{k})\hat{\rho}_M(x_1 + (\hat{\sigma} - \hat{\alpha})k_1)\Psi_\beta(x_1 - \hat{\alpha}k_1, \boldsymbol{\zeta})\right] d\boldsymbol{\zeta} \, d\boldsymbol{k} \, d\hat{\alpha}, \tag{C1d}$$

$$Q^{(v)}[\Psi_\beta] = \frac{1}{4\sqrt{2\pi}k} \int_0^{\hat{\sigma}} \iint k_2 \hat{Y}\left(\hat{\rho}_M\left(x_1 + \left(\frac{1}{2}\hat{\sigma} - \hat{\alpha}\right)k_1\right); \eta_0\right)$$

$$\times \left[I_Q^{(+)}(\boldsymbol{\zeta} \cdot \boldsymbol{k})\hat{\rho}_M(x_1 - \hat{\alpha}k_1)\Psi_\beta(x_1 + (\hat{\sigma} - \hat{\alpha})k_1, \boldsymbol{\zeta})\right.$$

$$\left. + I_Q^{(-)}(\boldsymbol{\zeta} \cdot \boldsymbol{k})\hat{\rho}_M(x_1 + (\hat{\sigma} - \hat{\alpha})k_1)\Psi_\beta(x_1 - \hat{\alpha}k_1, \boldsymbol{\zeta})\right] d\boldsymbol{\zeta} \, d\boldsymbol{k} \, d\hat{\alpha}, \tag{C1e}$$

where

$$r_A = x_1 - \hat{\alpha}z, \quad r_B = x_1 + (\hat{\sigma} - \hat{\alpha})z, \quad r_C = x_1 + \left(\frac{1}{2}\hat{\sigma} - \hat{\alpha}\right)z, \tag{C2a}$$

$$I_P^{(\pm)}(t) = \pi^{-1/2} \int_{\pm t}^{\infty} (\tau \mp t)^2 e^{-\tau^2} \, d\tau, \tag{C2b}$$

$$I_Q^{(\pm)}(t) = \pm\pi^{-1/2} \int_{\pm t}^{\infty} (\tau \mp t)^2 (\tau \pm t) e^{-\tau^2} \, d\tau. \tag{C2c}$$

The functions $(G_{11,P}^{(v)}, G_{22,P}^{(v)})$ and $P_{12,\omega_P}^{(v)}$ are respectively given by the definitions of $(G_{11,T}^{(v)}, G_{22,T}^{(v)})$ and $P_{12,\omega_T}^{(v)}$ with their respective last terms $\hat{Y}(\hat{\rho}_M(r_C); \eta_0)\hat{\rho}_M(r_A)\hat{\rho}_M(r_B)$ and $(\frac{1}{2}\hat{\sigma} - \hat{\alpha})\hat{Y}(\hat{\rho}_M(r_C); \eta_0)\hat{\rho}_M(r_A)\hat{\rho}_M(r_B)$ in the curly brackets being dropped and $\hat{\omega}_T$ being replaced by $\hat{\omega}_P$.

Appendix D. Information of computations

In this appendix, the information of computations is briefly described. The results shown in § 4 are those obtained with the molecular-velocity lattice system consisting of $336 \times 64 \times 64$ points in $\zeta_1\zeta_2\zeta_3$-space and the spatial lattice system consisting of 181 points. For ζ_1, the minimum lattice interval is 1.243×10^{-5} around $\zeta_1 = 0$, while the maximum interval is 0.0931 around $\zeta_1 = \pm 4.5$. For ζ_2 and ζ_3, the lattice interval is uniformly 0.369. For x_1, the minimum lattice interval is 5.242×10^{-5} around $x_1 = -1/2$, while the maximum interval is 6.944×10^{-3} around $x_1 = 0$ in the case of $\hat{\sigma} = 0$. In the case of $\hat{\sigma} \neq 0$, this arrangement is shrunk to the interval $[-(1 - \hat{\sigma})/2, 0]$. In the computation of the collision

962 A20-32

integral, $192 \times 64 \times 64$ modes in the frequency domain for $\zeta_1 \zeta_2 \zeta_3$-space and 32 and 16 Gauss–Legendre quadrature points for the polar and azimuthal angles of vector $\boldsymbol{k}$ (with the x_1 direction as the polar direction) are used. The results shown in figures 2–14 are those for which numerical convergence has been judged within the error invisible in the figures through the comparison with the results obtained with other lattice systems and parameters. The momentum conservation law (2.19) provides another measure of accuracy. The values of $|S_T|$ and $|S_P|$, which should theoretically be zero within the linearized regime, are bounded respectively by 6.0×10^{-6} and 3.0×10^{-5} for all values of k and $\hat{\sigma}$ chosen. This also supports the accuracy of the present computation.

REFERENCES

BIRD, G.A. 1994 *Molecular Gas Dynamics and the Direct Simulation of Gas Flows*. Clarendon.

CARNAHAN, N.F. & STARLING, K.E. 1969 Equation of state for nonattracting rigid spheres. *J. Chem. Phys.* **51**, 635–636.

CERCIGNANI, C. 1988 *The Boltzmann Equation and Its Applications*. Springer.

CERCIGNANI, C. & DANERI, A. 1963 Flow of a rarefied gas between two parallel plates. *J. Appl. Phys.* **34**, 3509–3513.

CERCIGNANI, C. & LAMPIS, M. 1988 On the kinetic theory of a dense gas of rough spheres. *J. Stat. Phys.* **53**, 655–672.

CERCIGNANI, C. & SERNAGIOTTO, F. 1966 Cylindrical Poiseuille flow of a rarefied gas. *Phys. Fluids* **9**, 40–44.

CHAPMAN, S. & COWLING, T.G. 1991 *The Mathematical Theory of Non-uniform Gases*, 3rd edn. Cambridge University Press.

DIMARCO, G. & PARESCHI, L. 2014 Numerical methods for kinetic equations. *Acta Numerica* **23**, 369–520.

EWART, T., PERRIER, P., GRAUR, I.A. & MÉOLANS, J.G. 2007 Mass flow rate measurements in a microchannel, from hydrodynamic to near free molecular regimes. *J. Fluid Mech.* **584**, 337–356.

FILBET, F., MOUHOT, C. & PARESCHI, L. 2006 Solving the Boltzmann equation in $N \log_2 N$. *SIAM J. Sci. Comput.* **28**, 1029–1053.

FREZZOTTI, A. 1997 A particle scheme for the numerical solution of the Enskog equation. *Phys. Fluids* **9**, 1329–1335.

FREZZOTTI, A. 1999 Monte Carlo simulation of the heat flow in a dense hard sphere gas. *Eur. J. Mech. B/Fluids* **18**, 103–119.

FREZZOTTI, A., BARBANTE, P. & GIBELLI, L. 2019 Direct simulation Monte Carlo applications to liquid-vapor flows. *Phys. Fluids* **31**, 062103.

FREZZOTTI, A., GIBELLI, L. & LORENZANI, S. 2005 Mean field kinetic theory description of evaporation of a fluid into vacuum. *Phys. Fluids* **17**, 012102.

FUNAGANE, H. & TAKATA, S. 2012 Hagen–Poiseuille and thermal transpiration flows of a highly rarefied gas through a circular pipe. *Fluid Dyn. Res.* **44**, 055506.

HASEGAWA, M. & SONE, Y. 1988 Poiseuille and thermal transpiration flows of a rarefied gas for various pipes. *J. Vac. Soc. Japan* **31**, 416–419 (in Japanese).

HATTORI, M. & TAKATA, S. 2015 Second-order Knudsen-layer analysis for the generalized slip-flow theory I. *Bull. Inst. Math. Acad. Sin. (N.S.)* **10**, 423–448.

HATTORI, M., TANAKA, S. & TAKATA, S. 2022 Heat transfer in a dense gas between two parallel plates. *AIP Adv.* **12**, 055220.

KOSUGE, S., SATO, K., TAKATA, S. & AOKI, K. 2005 Flows of a binary mixture of rarefied gases between two parallel plates. *AIP Conf. Proc.* **762**, 150–155.

LOYALKA, S.K. 1971 Kinetic theory of thermal transpiration and mechanocaloric effect. I. *J. Chem. Phys.* **55**, 4497–4503.

LOYALKA, S.K. 1975 Kinetic theory of thermal transpiration and mechanocaloric effect. II. *J. Chem. Phys.* **63**, 4054–4060.

LOYALKA, S.K. & HAMOODI, S.A. 1990 Poiseuille flow of a rarefied gas in a cylindrical tube: solution of linearized Boltzmann equation. *Phys. Fluids* A **2**, 2061–2065.

MALEK MANSOUR, M., BARAS, F. & GARCIA, A.L. 1997 On the validity of hydrodynamics in plane Poiseuille flows. *Physica* A **240**, 255–267.

MONTANERO, J.M. & SANTOS, A. 1996 Monte Carlo simulation method for the Enskog equation. *Phys. Rev.* E **54**, 438–444.

NIIMI, H. 1968 Thermal creep flow of rarefied gas through a cylindrical tube. *J. Phys. Soc. Japan* **24**, 225.

NIIMI, H. 1971 Thermal creep flow of rarefied gas between two parallel plates. *J. Phys. Soc. Japan* **30**, 572–574.

OHWADA, T., SONE, Y. & AOKI, K. 1989 Numerical analysis of the Poiseuille and thermal transpiration flows between two parallel plates on the basis of the Boltzmann equation for hard-sphere molecules. *Phys. Fluids A* **1**, 2042–2049.

SHAN, B., CHEN, S., GUO, Z. & WANG, P. 2021 Pore-scale study of non-ideal gas dynamics under tight confinement considering rarefaction, denseness and molecular interactions. *J. Nat. Gas Sci. Engng* **90**, 103916.

SHARIPOV, F. 1999 Non-isothermal gas flow through rectangular microchannels. *J. Micromech. Microengng* **9**, 394–401.

SHARIPOV, F. 2003 Application of the Cercignani–Lampis scattering kernel to calculations of rarefied gas flows. III. Poiseuille flow and thermal creep through a long tube. *Eur. J. Mech. B/Fluids* **22**, 145–154.

SHENG, Q., GIBELLI, L., LI, J., BORG, M.K. & ZHANG, Y. 2020 Dense gas flow simulations in ultra-tight confinement. *Phys. Fluids* **32**, 092003.

SONE, Y. 2007 *Molecular Gas Dynamics: Theory, Techniques, and Applications*. Birkhäuser, Supplementary Notes and Errata: Kyoto University Research Information Repository (http://hdl.handle.net/2433/66098).

SONE, Y. & YAMAMOTO, K. 1968 Flow of rarefied gas through a circular pipe. *Phys. Fluids* **11**, 1672–1678.

TAKATA, S. & FUNAGANE, H. 2011 Poiseuille and thermal transpiration flows of a highly rarefied gas: over-concentration in the velocity distribution function. *J. Fluid Mech.* **669**, 242–259.

TIJ, M. & SANTOS, A. 1994 Perturbation analysis of a stationary nonequilibrium flow generated by an external force. *J. Stat. Phys.* **76**, 1399–1414.

WU, L., LIU, H., REESE, J.M. & ZHANG, Y. 2016 Non-equilibrium dynamics of dense gas under tight confinement. *J. Fluid Mech.* **794**, 252–266.

WU, L., ZHANG, Y. & REESE, J.M. 2015 Fast spectral solution of the generalized Enskog equation for dense gases. *J. Comput. Phys.* **303**, 66–79.

ZHENG, Y., GARCIA, A.L. & ALDER, B.J. 2002 Comparison of kinetic theory and hydrodynamics for Poiseuille flow. *J. Stat. Phys.* **109**, 495–505.